Modeling and Simulation of Electromagnetic Retarder for Vehicle Application

Motuma Gezu Asfaw

A Thesis Submitted to the Department of Mechanical Engineering

School of Mechanical, Chemical and Material Engineering

Presented in Partial Fulfillment of the Requirement for the Degree of Master's in Automotive Engineering

Office of Graduate Studies

Adama Science and Technology University

May, 2024

Adama, Ethiopia

Modeling and Simulation of Electromagnetic Retarder for Vehicle Application

Motuma Gezu Asfaw

Advisor: Siraj Kedir Buse (Ph.D)

A Thesis Submitted to the Department of Mechanical Engineering

School of Mechanical, Chemical and Material Engineering

Presented in Partial Fulfillment of the Requirement for the Degree of Master's in Automotive Engineering

Office of Graduate Studies
Adama Science and Technology University

May, 2024

Adama, Ethiopia

DECLARATION

I hereby declare that this Master Thesis entitled "**Modeling and Simulation of Electromagnetic Retarder for Vehicle Application" is** my original work. That is, it has not been submitted for the award of any academic degree, diploma, or certificate in any other university. All sources of materials that are used for this thesis have been duly acknowledged through citation.

Name of student	Signature	Date

RECOMMENDATION

I, the advisor of this thesis, hereby certify that I/we have read the revised version of the thesis entitled "**Modeling and Simulation of Electromagnetic Retarder for Vehicle Application"** prepared under my/our guidance by **Motuma Gezu Asfaw** submitted in partial fulfillment of the requirements for the degree of Mater's of Science in Automotive Engineering. Therefore, I recommend the submission of a revised version of the thesis to the department following the applicable procedures.

______________________	________________	________________
Major Advisor	Signature	Date

APPROVAL

I, the advisors of the thesis entitled "**Modeling and Simulation of Electromagnetic Retarder for Vehicle Application"** and developed by **Motuma Gezu Asfaw,** hereby certify that the recommendation and suggestions made by the board of examiners are appropriately incorporated into the final version of the thesis.

______________________	________________	_______________
Major Advisor	Signature	Date

APPROVAL OF BOARD OF REVIEWERS

We, the undersigned, members of the Board of Examiners of the thesis by **Motuma Gezu Asfaw** have read and evaluated the thesis entitled "**Modeling and Simulation of Electromagnetic Retarder for Vehicle Application"** and examined the candidate during the open defense. This is, therefore, to certify that the thesis is accepted for partial fulfillment of the requirement of the degree of Master of Science in Automotive Engineering.

______________________	______________	______________
Chairperson	Signature	Date
______________________	______________	______________
Internal Examiner	Signature	Date
______________________	______________	______________
External Examiner	Signature	Date

Finally, approval and acceptance of the thesis are contingent upon the submission of its final copy to the Office of Postgraduate Studies (OPGS) through the Department of Graduate Council (DGC) and School Graduate Committee (SGC).

______________________	______________	______________
Department Head	Signature	Date
______________________	______________	______________
School Dean	Signature	Date
______________________	______________	______________
Office of Postgraduate Studies, Dean	Signature	Date

ACKNOWLEDGMENT

My sincere gratitude goes out to Dr. Siraj Kedir Buse, who served as my thesis advisor, for leading me through the process and providing me with insightful advice, motivation, and helpful criticism. I appreciate the chance to work with such a committed mentor since their knowledge, understanding, and support have been vital to me.

I would like to take this chance to convey my sincere gratitude to everyone who has helped me finish my thesis, Modeling and Simulation of Electromagnetic Retarder for Vehicle Application. My family and friends deserve special recognition since they have provided unwavering support, inspiration, and motivation throughout the journey.

ABSTRACT

Electromagnetic retarders in vehicles have become increasingly popular over the years. These devices control the speed of vehicles during braking, providing a safe and reliable means of deceleration. An electromagnetic retarder is described in this study as an additional braking device for conventional friction brakes to increase efficiency and service life. The main aim of this study is to model and simulate an electromagnetic retarder for vehicle application. An accurate and reliable mathematical model is evaluated for an electromagnetic retarder and controllers such as FLC and PSO are utilized and its performance is explored through simulations using MATLAB software. The settling time for the Fuzzy Logic Controller is 7.5 seconds, while for the PSO it is 3.5 seconds; additionally, the peak overshoot is 30% with the Fuzzy Logic Controller and 12% with PSO. The findings revealed that the EMR employing the PSO-based controller exhibited faster settling times compared to the EMR utilizing a fuzzy logic controller, along with a reduced peak overshoot value. For the same speed change value, the PSO controller-based EMR demonstrates the highest EM current and, consequently, the greatest braking torque resulting in superior braking performance. The study showcases the potential for the controllers to advance electromagnetic retarder braking technology, offering promising prospects for safer and more efficient braking systems. Overall, the study contributes to advancing electromagnetic retarders for vehicle applications.

Keywords: Electromagnetic retarder, Fuzzy logic controller, PSO

TABLE OF CONTENTS

LIST OF FIGURES

LIST OF TABLES

LIST OF ACRONYMS

CFD - Computational Fluid Dynamics

ECBS - Eddy Current Braking System

EHR - Eddy Current-Hydraulic Hybrid Retarder

EMR - Electromagnetic retarder

FEA - Finite Element Analysis

FIS - Fuzzy inference system

FLC - Fuzzy Logic Controller

NSGA-II - Non-Dominated Sorting Genetic Algorithm-ii

PSO - Particle Swarm Optimization Controller

PWM - Pulse Width Modulation

FEM - Finite Element method

1. INTRODUCTION

1.1. Background of the study

EMR are becoming increasingly popular in vehicles, particularly heavy-duty vehicles such as buses and trucks. They are also used in passenger cars, such as hybrid and electric vehicles. Electromagnetic retarders (EMR) use electromagnetic forces to slow down a vehicle (Kimbrough, 2018). They are typically used with traditional friction brakes to provide a more efficient and reliable braking system. EMR work by using the interaction of magnetic fields to generate friction (Wu et al., 2009). EMR is used as a supplementary braking system with the conventional friction brakes so that they can operate less frequently. This can lead to increased braking efficiency, reduced wear and reduced emissions. EMR are also more reliable because they do not wear out as quickly as friction brakes and this can lead to lower maintenance costs A rotating metal disc passes through a stator, a set of electromagnets. The stator creates a magnetic field that interacts with the magnetic field of the rotating metal disc due to the creation of eddy current, which causes the shaft to slow down (Hu, 2012).

The following are some of the potential benefits of EMR:

- Improved fuel economy and reduced emissions
- Increased reliability and reduced maintenance costs
- Improved safety by providing a more reliable braking system

As a result, modeling and simulation of electromagnetic retarders have become essential research areas in vehicle engineering. This paper aims to provide modeling and simulation of electromagnetic retarders for vehicle application, highlighting the current trends, challenges, and opportunities (Sirumalla et al, 2022)

Electromagnetic retarders have several advantages over other brakes, including hydraulic and pneumatic ones. The electromagnetic retarder is quieter and requires less maintenance than its hydraulic and pneumatic counterparts. It can also be integrated with other vehicle systems, such as regenerative and anti-lock braking systems, to improve the vehicle's performance (Shreyansh et al, 2022).

Modeling and simulating electromagnetic retarders are necessary to predict their performance, design parameters, and control strategies. Over the years, different modeling techniques have been developed to simulate the behavior of electromagnetic retarders. These techniques range from analytical and numerical methods to experimental testing (Talaat, 2014).

Analytical modeling uses mathematical equations to describe the behavior of the electromagnetic retarder. These models are usually based on physical principles such as Lenz's Law and Faraday's Law of Electromagnetic Induction. They provide accurate results with minimal computational effort and can be used to optimize the design parameters of the electromagnetic retarder. Numerical modeling involves using computational methods to simulate the electromagnetic retarder's behavior. These methods include computational fluid dynamics (CFD) simulations and finite element analysis (FEA) (LIU ,2008).

Several challenges exist in modeling and simulating electromagnetic retarders for vehicle applications. One of the significant challenges is accurately modeling the electromagnetic brake's behavior, which involves the interaction of several physical variables such as magnetic field strength, air gap distance, and braking force. Another challenge is dealing with the non-linear and time-varying behavior of the electromagnetic retarder. This behavior can change under different operating conditions, such as temperature, speed, and load conditions, requiring adaptive control strategies.

Despite these challenges, modeling and simulation of electromagnetic retarders continue to present opportunities for improving the performance and efficiency of vehicles, leading to reduced emissions and enhanced safety. The development of more accurate models and control strategies will not only improve the performance of the electromagnetic retarder but also reduce the time and costs associated with experimental testing (Routh et al., 2008).

In general, the modeling and simulation of electromagnetic retarders for vehicle applications is a critical research area that can potentially improve vehicle performance, energy efficiency, and safety. Analytical, and numerical approaches have been developed for modeling and simulating the electromagnetic retarder's behavior. Despite the challenges associated with accurately modeling the electromagnetic retarder's behavior, continued research is necessary to achieve more accurate models and control strategies for vehicles that use electromagnetic retarders.

1.2. Statement of the problem

The transportation sector is going through a radical change as it moves toward efficient and sustainable technology, with an increasing focus on electric and hybrid cars. The electromagnetic retarder, a vital mechanism intended to improve brake efficiency and overall vehicle safety, is one of the major elements advancing modern technologies. Notwithstanding its importance, there is still a deficiency in our knowledge and thorough modeling of electromagnetic retarders, especially when it comes to automotive applications (Ding et al., 2023).

The complex nature of the system's interactions is frequently not sufficiently captured by current models, which makes it difficult to forecast real-world performance with precision. Thus, potential gains in energy efficiency and safety that these systems might provide face challenges in the optimisation and improving of electromagnetic retarders for particular vehicle applications.

Furthermore, as the automotive industry increasingly embraces electrification, there is a pressing need for advanced simulation tools that can accommodate the unique characteristics and demands of electromagnetic retarders in electric and hybrid vehicles. The integration of these systems with diverse propulsion technologies requires a comprehensive understanding of their behavior under various operating conditions, which is currently insufficiently addressed in the literature (Hu, 2012).

This study aims to address these critical gaps by developing an advanced and comprehensive model for the modelling and simulation of electromagnetic retarders specifically tailored for vehicle applications. The research investigated the intricate electromagnetic, and mechanical interactions within the retarder system, seeking to enhance the accuracy and versatility of existing models. Through a systematic approach, the study aims to provide valuable insights into the optimization of electromagnetic retarders for diverse vehicle platforms, contributing to the ongoing efforts to advance sustainable and efficient transportation technologies.

1.3. Objectives

1.3.1. General objective

The general objective of this study is modeling and simulation of electromagnetic retarders for vehicle application.

1.3.2. Specific objectives

The specific objectives were as follows:

- To evaluate mathematical model for the proposed electromagnetic retarder.
- To examine existing control mechanism for electromagnetic retarder.
- Perform simulations to analyze electromagnetic retarders control parameters.

1.4. Significance of the study

The research's outcomes would make a significant contribution to improving electromagnetic retarders in vehicles, particularly in heavy-duty vehicles, in order to increase efficiency, reduce wear, and improve service life. Evaluating a mathematical model and perform simulation of an electromagnetic retarder will provide a valuable tool for engineers and researchers in this field. The simulation results will help to improve the retarder's design and optimize its performance, leading to improved vehicle safety and reliability.

1.5. Scope of the study

This study delimited only on the Modelling and Simulation of Electromagnetic retarders for vehicle application. Evaluating a mathematical model of an electromagnetic retarder that is accurate and reliable. Also Perform simulations to analyze electromagnetic retarders control parameters.

1.6. Organization of the study

This study was organized into six chapters. Chapter 1 gives the Introduction of the study. The introduction provided a brief overview of the topic of the electromagnetic retarder, including the background, objectives, and significance of the study.

Chapter 2 is Literature Review: The literature review discussed the previous research that has been conducted on electromagnetic retarders. The review focused on the mathematical modeling and simulation of electromagnetic retarders.

Chapter 3 is Materials and Method: The mathematical model is evaluated in this chapter by identifying the mathematical equations considering several key design variables that govern the operation of the electromagnetic retarder.

Chapter 4 is the Result and Discussions: The simulation result of the electromagnetic retarder control parameters is analyzed and existing control mechanism for the electromagnetic retarder is examined in this chapter. The results of the simulation is presented and discussed to improve the electromagnetic retarder's performance.

Chapter 5 gives a Conclusions and Recommendations: The conclusion summarized the main findings of the research and discuss the implications of the research for the design and optimization of electromagnetic retarders. Future research direction is recommended to enhance both the performance and controllability of the electromagnetic retarder.

2. LITERATURE REVIEW

Several studies have recently conducted on the vehicle's electromagnetic brake retarder. This section summarizes the research that have been most useful in addressing various areas of this study. Also, the chapter provides an overview of the literature on electromagnetic brake retarder modelling, simulation, and analysis. The research gap is addressed at the end of this chapter.

2.1. Working principle of Electromagnetic Retarder

Electromagnetic retarder works on Faraday's law of electromagnetic induction to generate an electromagnetic field. When the vehicle or the train's rotor rotates in this field's magnetic influence, the retarding effect generates forces that result in braking. The electromagnetic retarder has better control over speed than the traditional braking system (Reverdin & Borione, 1974).

The electromagnetic retarder works by creating Eddy currents within a revolving metal disk between two electromagnets, creating a force that opposes the rotation. due to the change in magnetic field within the disk that opposes the magnetic field of the retarder (Wu et al., 2009). If the magnetic is not energized, the disc rotates freely and accelerates uniformly due to the weight of the shaft. When the electromagnet is activated, the spinning of the disc is slowed, and the energy absorbed manifests as heating of the disc The electromagnetic current is adjusted using a Rheostat when the brake pedal is applied. This provides total control of the torque of the electromagnetic retarder by altering the DC current to the electromagnet (Shreyansh et al, 2022)

Eddy currents in a conductor move on a plane transverse to the magnetic field, forming closed loops. According to Lenz's law, eddy currents generate a magnetic field perpendicular to the source's magnetic field. Eddy currents within a conductor generate a magnetic field with the opposite polarity as the externally applied field (Sirumalla et al, 2022).

2.2. Modeling and Design of Electromagnetic Retarder

LEE, (2012) paper is about developing and testing an electromagnetic retarder for automobile use. The literature review section of the paper covers previous research on electromagnetic retarder brakes and retarders, including their principles of operation, design considerations, and applications in various industries.

Enokizono et al. (2001) present the design of a retarder with permanent magnet-type by using FEM with an upwind interpolation function. The paper describes the equation of motion for the analysis of the deceleration process of the conductive plate. The numerical result obtained describes the arrangements of suitable permanent magnet and the constructions of the yoke. The paper is a valuable contribution to the field of electromagnetic retarder design and provides useful insights for future research in this area.

Chengye & Jianming (2013) discuss the key technologies in designing electromagnetic retarders used as auxiliary braking devices in top-grade buses and heavy-duty vehicles. The paper analyzes the electromagnetic retarders working principles and its structure, including the rotor disk's magnetic circuit, material selection, and blade design. The paper also discusses the advantages of electromagnetic retarders, including their impact on braking performance, power consumption, weight, and stability. The paper provides an overview of the design technologies involved in electromagnetic retarders and their application in the automotive industry.

LIU (2008) presents a comprehensive study on the unsteady thermal field of a rotor plate used in electromagnetic retarders for automobiles. Using a physical model based on the virtual boundary method and heat transfer theory, the authors establish the finite element governing equation using the Galerkin, which is stable under any condition. The study also introduces a new style of varying time step method used in the iteration process. The authors analyze the thermal field on the rotor plate in both the axle and radial directions and measure the temperature variation at specific points on two side-surfaces. The data obtained through analytical and testing procedures are uniform and provide valuable insights for the initial design stage of the electromagnetic retarder using the FEM.

Figure 2.1 displays the finite element modeling (FEM) of one pole of the EMR. Just one Pole was considered to reduce the amount of computation required. The method was used on a high-speed train's EMR, and the resulting braking forces were compared to measurements. Electromagnetic brakes or EMBs, stop electrical machine rotors. The force parameters of an EMB employing co-energy and just considering the primary flux connection was determined using the Finite Element Method (FEM) (Ha et al., 1999).

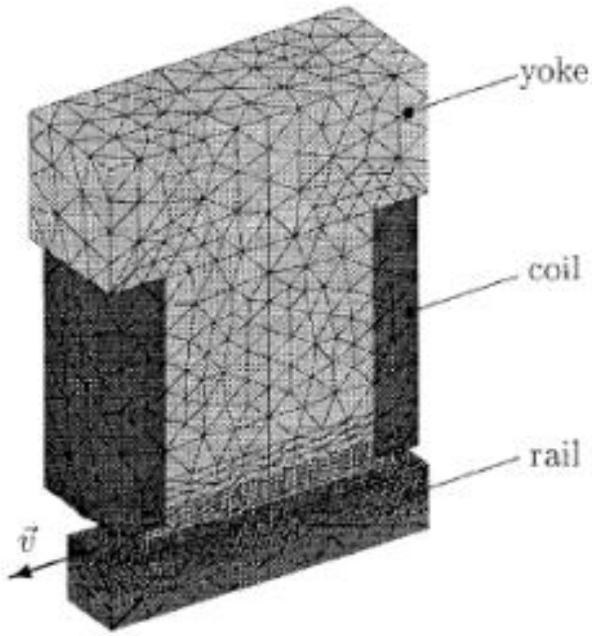

Figure 2.1. Longitudinal section view of a pole of an EMR (Albertz et al., 1996)

The 3-D FEM approach can be used to improve brake performance. This method helped to acquire the brake's optimal geometry. Finite elements could be used to solve 3-D and 2-D electromagnetic retarder problems. Given that magnetic properties are temperature-dependent, a water-cooled PM-type EMR might be designed using a FEM. Water cooling assisted in achieving a low working temperature. Consequently, better braking efficiency was attained (Ye et al., 2011).

Since the PM EMR does not require an electric control unit or a power supply, it does not require an electric circuit. Using a permanent magnet material makes the design lightweight and compact. A magnet-type axial flux (AFPM) and a permanent magnet (RFPM) type radial flux machine are the two types of PM-EMR. Another name for this sort of gadget is the AFPM. As seen in Figure 2.2, it offers the advantage of simple brake energy management by adjusting the mechanical air gap. Analytical field computing was used to analyze the braking torque, and 3-D FEA was used to validate the findings. Electrical control is used to operate electromagnetic retarder brakes. The torque that the EMR generates at low speeds is inadequate. Research has been done on the effectiveness of employing a variable frequency magnetic field with different waveforms, such as square and saw tooth, to address the issue of inadequate torque (Lubin & Rezzoug, 2017).

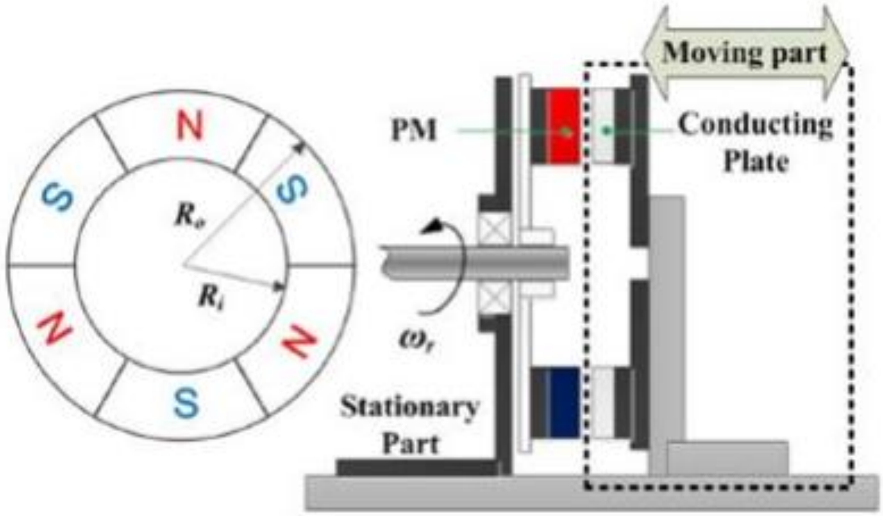

Figure 2.2. Axial PM type EMR (Lubin & Rezzoug, 2017)

Using dc and ac magnetic fields on an analytical model, the effects of the results were verified with the aid of FEA. The braking torque reference value determined using a DC field was used. The findings led to three primary conclusions. First, it was determined that the characteristic of the applied external field was crucial to the EMR braking performance. Second, braking torque was obtained at lower frequencies with a greater value. The pace at which the applied field changes affects the braking torque. The rate of wave change determines the braking torque when various waveforms are applied at the same frequency. Thirdly, the braking torque for all waveforms reduces as frequency increases (Karakoc et al., 2016).

2.3. Application of electromagnetic retarder

Electromagnetic retarders are primarily used in heavy-duty vehicles and can slow down or stop large vehicles without relying solely on the vehicle's brakes. Some typical applications of electromagnetic retarders include trucks and buses, construction vehicles and rail transportation.

Tian et al. (2020) discuss designing and testing an electromagnetic retarder -hydraulic hybrid retarder (EHR) for heavy-duty vehicles. Heavy-duty vehicles rely on non-contact hydraulic or electromagnetic retarders to ensure safe driving on downhill terrain. However, each type of retarder has limitations - hydraulic retarders generate large torque at high speeds but struggle at low speeds, while electromagnetic retarders have the opposite issue. Fortunately, the braking performances of these two retarders complement each other well. That's where the electromagnetic -hydraulic hybrid retarder (EHR) comes in. By combining the principles of electromagnetic and hydraulic braking, EHRs offer a solution that takes advantage of the strengths of both types of retarders. The design of the EHR involves utilizing both sides of the rotor for hydraulic braking and generating electromagnetic retarders in the outer ring of the rotor. Computer simulations were used to predict the braking torque of the EHR, and bench tests were performed on the prototype to evaluate its performance. The results showed that the EHR relies on electromagnetic retarder braking at low speeds and a combination of electromagnetic retarder and hydraulic braking at high speeds. Best of all, the EHR's control system is simple - it can be adjusted solely by tweaking the braking torque of the electromagnetic retarder component.

Pandey et al. (2015) provide an overview of the use of retarders as a supplementary braking system in heavy vehicles. The paper highlights the limitations of friction-based braking systems, which results in brake fade when it’s used continuously. Conversely, retarders used to slow down or maintain a steady speed to prevent the vehicle from accelerating down the decline. It also discusses two types of retarders - hydraulic and electric. Hydraulic retarders use the viscous drag forces between dynamic and static vanes in a fluid-filled chamber to achieve retardation. Electric retarders, on the other hand, use electromagnetic induction to provide a retardation force. The authors also discuss the installation of retarders, which can be done offline or inline. Offline installation involves attaching the retarder to the transmission, with the prop shaft remaining unmodified and the auxiliary power take-offs freely accessible. Inline installation, on the other hand, involves attaching the retarder to the transmission and using its oil supply system. This method is perfectly suitable for retrofitting

2.4. Electromagnetic retarder and Electromagnetic retarder brakes

A circular current formed on a disc or conductor when a magnetic field changes. The current follows Lenz's law, moving in a way that opposes the change in the magnetic field. If a constant magnetic current cuts a moving conductor's surface, counter-top currents are induced near the polar projection region (Karakoc et al., 2016). These currents create a braking torque due to their interaction with magnetic flux. Eddy current flows in circular paths close to the magnetic field, giving them their name. They generate a force that opposes the conductor's motion as they interact with the magnetic field. Eddy current is also known as Foucault currents after their discoverer, and they only occur when a conductive material moves relative to an external magnetic field. To generate energy, either a moving conductor and stationary ground or a moving field and stationary conductor must be present (Aguiar et al., 2009).

Simeu & Georges (2016) Electromagnetic retarder, due to their tendency to restrict the source of their origin, result in energy loss. This is viewed as unnecessary in appliances such as transformers and rotating machines. However, electromagnetic retarder brakes (EMR) utilize these losses for operation. The principle behind EMR is based on Faraday's law of induction, which states that when a conductor moves through a constant magnetic field, an induced current is generated, producing a force that opposes the motion of the conductor. An EMR comprises an aluminum disc driven by a motor in continuous rotational motion through an electromagnet air gap, but electromagnetic retarder braking can also occur in a thin metal strip. The magnetic induction caused by electromagnetic retarder is insignificant at low speeds compared to the original. EMR behave like a linear damper because the braking force derived from the induced magnetic field is directly proportional to the speed. The induced eddy current creates a repulsion force proportional to the conductor's speed. Therefore, the conductor and its motion act like a viscous damper. EMR provide linear and programmable physical damping, making them ideal for use as dissipative actuators.

The PM-type ECR is a useful additional braking system for heavy vehicles such as trucks, especially when driving down a long slope (Zhang et al., 2014). It offers the benefits of being simple and compact, and its magnetic field does not require any extra power supply, unlike an ECR-type electromagnet. The two main components of this type of ECR are the stator, which is attached to the back and features many magnets that produce a powerful magnetic field, and the rotor, which is made of a steel ring with blades. When the brake is turned off, all the magnets are in a position where they only complete the magnetic circuit of the poles. However, when the brake is turned on, the magnetic circuit changes and the magnets complete a path through the poles to the rotor, thus generating electromagnetic retarder s inside the rotor, which act as a braking force. The temperature can impact the braking performance, and the material and structure of the rotor can affect the braking force produced. A parametric model and a parameter estimation method were developed to enhance the effectiveness of this type of ECR for automotive braking applications (Ye et al., 2019). A car's braking system holds immense importance, and ECR intends to manufacture a superior and upgraded system to replace the current hydraulic model. This novel system offers enhanced performance and control while promoting an eco-friendly solution. Research suggests that an eddy-current methodology can yield the desired outcomes.

2.5. Design consideration and performance characteristics of EMR

To reduce the computational effort, only one pole was considered. The process was utilized to assess the EMR of a high-speed train and compare the resulting braking forces with the actual measurements. Electromagnetic brakes (EMBs) are implemented to decelerate the rotors of electrical machines. The co-energy approach was adopted using the FEM to determine the force features of an EMB, taking into account only the main flux linkage (Hadziselimovic et al., 2008). Overall braking performance and design optimization to decrease volume and enhance braking torque can be assessed using the 2D FEM.

The phenomenon of electromagnetic retarders holds great significance in analyzing electromagnetic devices such as electromagnetic retarder brakes (EMR). The magnetic equivalent circuit has been widely employed as a modeling technique to analyze electromagnetic retarder s by considering them as a source of magneto-motive force within a conductor. Additionally, this approach has been used extensively to evaluate the braking force generated by electromagnetic retarders. Notably, applying this method to analyze electromagnetic retarders in EMR has yielded favorable results. Therefore, it can be inferred that this approach could be considered for analyzing similar electromagnetic devices, such as solid rotor machines. Hence, the magnetic equivalent circuit is a promising modeling technique for evaluating electromagnetic retarder s in numerous electromagnetic devices (Gholizad et al., 2009).

The EMR, or electromagnetic retarder brake, has been studied extensively using mathematical modeling. One approach involved using principles from magnetic circle theory and antimagnetic force to develop a comprehensive model (Zhou et al., 2015). Another method utilized the Fourier transform to calculate the braking torque of the EMR. In certain instances, using a short primary scheme with a sheet secondary is more convenient and produces desirable results like those achieved with a brief primary lim. The inputs and outputs of the EMR impact the braking force and must be considered. A double-sided EMR with a short primary side can be compared to a double-sided lime and requires a narrow air gap thickness for optimal force generation. These models were developed through 2-D analytical calculations and demonstrated the effectiveness of the EMR in inducing eddy currents due to changing magnetic field generation. The EMR is composed of a multi-pole hetero-polar structure consisting of a conductive disc and multi-pole windings, both of which were considered when determining variations in brake geometry flux density and dc excitement current in analytical calculations (Srivastava & Kumar, 2009).

A computer analysis of the EMR in electric machines was conducted using the formula for braking force, considering the pole's actual width. The formula was applicable for both thick and thin discs over a wide range of speeds. An analytical solution was obtained to obtain total braking power. A mathematical analysis of the problem was conducted using a new expression of the braking forces obtained by solving the 2-D field problem of multiple regions with different permeability. A computer program calculated the braking force and observed the effect of harmonics at different speeds (Kado, 2009).

The skin effect affects the torque-speed characteristics of the cylindrical EMR, as seen in Figure 2.3. It was discovered during experimental studies examining two types of rotors—one with a steel core and the other with a bronze core—that the skin effect impacted the cylindrical EMR's performance. The skin effect and the armature reaction were the two main aspects that affected the electromagnetic retarder brake’s performance. The armature reaction was considered in several analytical alternatives, but the skin's impact on the braking torque velocity features was overlooked. It was possible to analyze the torque speed of the EMR with a cylindrical rotor while accounting for the armature's response and the skin effect.

Consequently, it is possible to determine critical speed and peak brake torque over a range of rates with the least error. Using EMR, a pendulum in a laser marker was subjected to damping analysis. In addition to two-dimensional motion analysis, electromagnetic retarder analysis was conducted using the three-dimensional FEM. The comparison of the measured and computed 2-D pendulum damping trajectory findings validates the value of the suggested approach (Sharif et al., 2012).

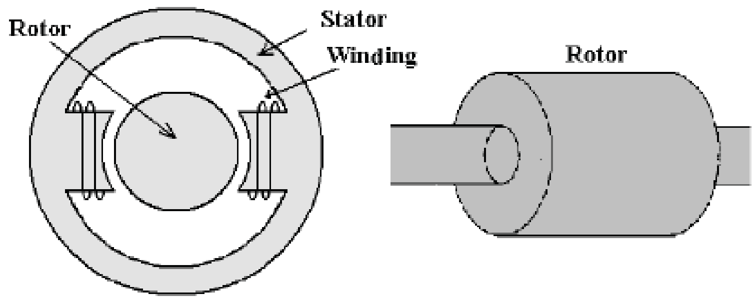

Figure 2.3. Simplified schematic diagram of a cylindrical EMR (Sharif & Sharif, 2009)

3D FEM was used in the investigations to see how the design of the slit affected the EMR's performance. Slit structure lowers the braking torque by increasing the disk's effective resistance. Figure 2.4 displays the whole EMR model in use, while Figure 2.5 displays a partial model with just one pole. The periodic condition can reduce the number of poles in this model (Ihm et al., 2008).

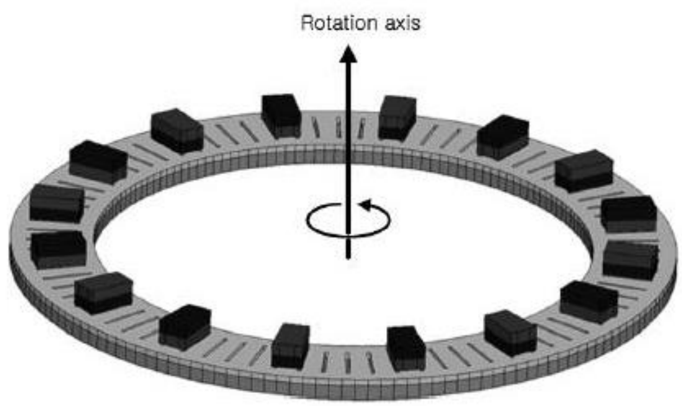

Figure 2.4. The geometry of the 3D FEM full model (Ihm et al., 2008)

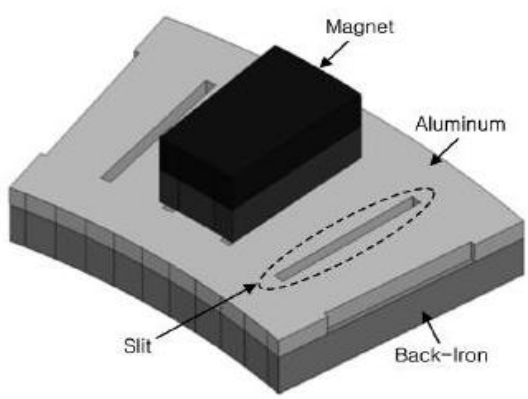

Figure 2.5. Simulated 3D partial model (Ihm et al., 2008)

It is possible to model an EMR using MATLAB. This model measured the brake's characteristic curves depending on its design, size, and usage materials. The characteristic curve changed as the model's parameters changed. Coefficients to modify the brake's equation's parameters were obtained using a finite element analysis (FEA) of the brake. The prototype and model's results were contrasted. The impact on the torque-speed curve design parameters of the EMR was examined using three-dimensional FEA. Using FEM, the phenomenon of magnetic flux density was examined under various air gap and track material conditions. The results acquired may prove useful in constructing the magnetic braking system. Using 3-D FEA, a parametric analysis of the axial flux wound-excitation EMR was carried out. The created FEA was used to validate the FEA results. Different ECR speeds produce different braking torques. The liquid-cooled electromagnetic retarder was presented as a solution to the thermal recession problem and as a means of energy conservation. A mathematical model was created and applied to the ECR's design (Liu et al., 2011).

A high-speed train's braking system is crucial to the vehicle's safety. Hardware in a loop system was created to analyze the features of Korea's high-speed train braking system. Verification of design characteristics and specifications was also done. An EMR's working speed range could be expanded by combining an EMR with a magnetic brake. Numerous benefits, including high force density, low cost, low loss, high reliability, and easy control, are associated with hybrid excitation linear EMR. A hybrid brake with electromagnetic retarder and electro-hydraulic components could address issues with wear, poor reaction, and heat failure of traditional EMR. It was discovered through experimental research that the performance of the hybrid brake was as intended (Kou et al., 2014).

2.6. Existing modeling and simulation approach of EMR

Niu et al. (2022) this paper explores the potential of using a permanent magnet electromagnetic retarder as a new type of vehicle auxiliary braking system. The study uses a combination of the non-dominated sorting genetic algorithm-ii (NSGA-II) and linear layer analysis method to optimize the device's parameters. The study establishes a mathematical optimization model of the permanent magnet electromagnetic retarder using the radial length, the thickness and the number of permanent magnet and the conductor disk thickness as the design variables, with optimization objectives of eddy current loss and the braking torque.

The NSGA-II algorithm then optimizes the device's braking torque and electromagnetic retarder loss. The result shows that the layer analysis model-based NSGA-II algorithm is more effective in optimizing the device's structural parameters than the standard genetic algorithm.

Niu et al. (2022) discuss the problem of heavy-duty vehicles decelerating on a long downhill and propose a solution using an electromagnetic retarder. The authors designed and tested a closed-loop pulse width modulation (PWM) braking controller to decelerate the vehicle and stabilize the speed at a desired value. The experiments showed that the constant speed running engine was decelerated in a controlled manner according to set-point values with a 4% steady-state error. The paper provides a detailed description of the experimental setup, the control system design, and the experiment results. The authors conclude that the proposed system can be applied easily to EMR of vehicles and can effectively stabilize the speed of heavy vehicles on long downhill runs.

Busher & Horoshko (2019) discusses the modeling and control of a system for adjusting the internal combustion engine of a car using retarders instead of wheels. The system includes an induction motor, a differential, and two retarder control systems. The control systems stabilize the speed of the axles using a single-loop system with a PI-speed controller for the left axle and a double-circuit system with a PI-speed controller and a relay current regulator for the right axle. The paper also discusses the non-linear dependence of the moment of the induction brake on the speed and current. It proposes using fractional-integral regulators for automating the tuning process. The paper concludes by stating that the final decision on the structure of the regulators will be made after testing the control system.

An EMR's design and optimization for various design parameters were shown. The magnetic and electric field modules of COMSOL Multi-physics were used for the simulation. A simulation was run to confirm the real outcomes. The study's initial parameters were loaded. An assessment of the electromagnetic retarder produced in the disc was carried out in a stationary investigation. A time-dependent investigation was also carried out to demonstrate the development of identical electromagnetic retarder s in the disc with deceleration. Electromagnetic retarder brakes are designed, analyzed, and torque-controlled optimally to decrease stopping distance while preserving the appropriate slip ratio that produces the most stopping force. For the best torque control, a sliding mode controller was mentioned (Lee & Park, 1999).

2.7. Research gap

It was discovered that while much work had been done on electromagnetic retarders (EMR) for heavy-duty vehicles as a supplementary braking system to slow down the vehicle, very little work had been done on the optimisation of electromagnetic retarders for diverse vehicle platforms, contributing to the ongoing efforts to advance sustainable and efficient transportation technologies.

3. MATERIALS AND METHODS

3.1. Materials

The software’s used in this study were

- MATLAB: Used to perform simulations to analyze electromagnetic retarders control parameters and to evaluate existing control mechanism of fuzzy logic control.

Material used for electromagnetic retarder is based on the Telma electromagnetic retarder specifications designed for different vehicle applications.

3.2. Methods

3.2.1. Mathematical Modeling of Electromagnetic Retarder

This chapter delves into the mathematical representation of an electromagnetic braking system. Establishing a mathematical model for the brake facilitates control and simulation purposes.

Maxwell's principles can be applied to the existing physical configurations to characterize the structural characteristics of an electromagnetic brake. This system involves a ferromagnetic disc with a permeability denoted as μ and electric conductivity, which is set in rotation atop a circular arrangement of rotating compressive poles. Each of these poles induces a magnetic excitation current, signified as "o," when the center of the disc is unsaturated. This excitation current is equivalent to the excitation flow within the unit. The magnetic flux forms loops established in the narrow gap between the discs and the poles. As the disc rotates, the magnetic flux experiences sinusoidal variations over time, as Equation (3.1) describes.

$$\varphi = \varphi_O \sin \frac{pN}{60} t \tag{3.1}$$

Where:

p = pole pair number
N=disc revolutions per minute
t = time in seconds

The rotating disc generates alternating currents in direct proportion to the magnetic flux. These currents circulate along the magnetic field lines, creating electromagnetic retarder that leads to heat production due to the disc material's electrical conductance (μ). When a magnetic system is rotated close to a conductive sheet along the normal axis, it initiates a braking torque on the system, which correlates directly with the angular velocity of the eddy current induced. The magnitude of the braking torque depends on the strength of the current and the magnetic flux.

3.2. Available Models

Within the scholarly discourse concerning electromagnetic retarder s, Smythe (1942), Schieber (1974), and Wouterse (1991) have each put three distinct methodologies. These methodologies represent varied approaches to addressing the underlying issue.

3.2.1. W.R. Smythe's Model

Smyth's approach addressed the problem by treating it as a torque calculation issue focused on a disc, employing a reflection technique to derive a comprehensive method for torque calculation. This method was specifically tailored to the problem's geometry, involving a couple of images capturing the standard velocity of the magnetic field due to electromagnetic retarder s emerging from both sides of the field. In the initial phase of the procedure, the calculation centered on the B magnet torque generated by the electromagnetic retarder s induced by a long, circular-shaped central portion within a rotating disc. Electromagnetic retarder s were generated by fluctuations in the outer region's magnetic field and variations in the magnetic distribution of the electromagnetic retarder s throughout the surrounding envelope. The torque could be computed by integrating the radial component of the current, factoring in the interaction between the magnet and the lever arm, and encompassing the edge region. This integration was performed across every cross-section of the rotating disc, considering the stream function of the point flowing from bottom to top. Due to a demagnetizing effect, the flux of the electromagnetic retarder experiences reduction due to interchangeable parts of the electromagnetic panel. If we denote φ_o as the flux penetrating the stationary disk, T as the brake torque, ω as the angular velocity, D as a constant coefficient, β as another constant coefficient, and γ as equal to 10^-9/ρ where ρ represents the disc's volume resistivity, the total flux when the disk is in motion would be determined.

$$\varphi = \varphi_o - \frac{\beta^2\gamma^2\omega^2\varphi}{R} = \frac{R\varphi_o}{R+\beta^2\gamma^2\omega^2} \tag{3.2}$$

And $\frac{\beta^2\gamma^2\omega^2\varphi}{R}$ it reflects the demagnetization flux achieved by dividing the electromagnet's reluctance of the demagnetizing MMF force. The ultimate brake torque integration result is

$$T = \omega\gamma\varphi^2 D = \frac{\omega\gamma R^2 {\varphi_o}^2 D}{(R+\beta^2\gamma^2\omega^2)^2} \quad (3.3)$$

This design exhibits an appealing aesthetic when operating at lower velocities, yet it experiences a notably rapid reduction in torque as speed increases. Smythe has astutely observed that this phenomenon could be ascribed to additional factors, such as the saturation level of the magnet's iron core, causing an interference with the mutual magneto motive force (MMF) and flux relationship. This, in turn, may necessitate adjustments to equations (3.2) and (3.3).

3.2.2 D. Schieber's Model

Schieber has created a general rotation scheme solution technique that differs from Smythe's approach (Karakoc et al., 2016). The result was:

$$T = \frac{1}{2}\sigma\delta\omega\pi r^2 m^2 {B_z}^2 \left[1 - \frac{\left(m/_R\right)^2}{\{1-(r/R)^2\}^2}\right] \quad (3.4)$$

Where

σ = electrical conductivity of rotating disc

δ = rotating disk sheet thickness

ω = angular velocity

m = electromagnet radius

r = distance between the disc center and the pole center projection area

R = radius of the disk

B_z = density of z-component of magnetic flux, z-axis is the direction of the electromagnetic pole center

This configuration is exclusively accessible at low velocities. Schieber observed that the outcomes he presented closely mirrored those reported by Smythe and applied to both linear and rotating strips. However, it should be noted that Schieber's investigations have not extended into the realm of high-speed conditions.

3.3.3. J.H. Wouterse's Model

Wouterse's endeavor involved seeking an alternative global torque solution within both the High-Speed and Low-Speed Regions, drawing inspiration from Schieber and Smythe's work. He observed that the electric field generated by the eddy brake's disk, denoted as E=nXB, is induced in parallel to both the tangential velocity of the rotating disk, represented by μ and the magnetic coil's magnetic field, denoted as B. When the velocity is considerably lower than the critical velocity at which maximum torque is produced, the current model's induction becomes relatively negligible compared to the initial magnetic field strength at null velocity, denoted as B_o. Considering these findings, Wouterse provided the mathematical framework for lower-speed scenarios (Pandey et al. 2015).

$$F_e = \frac{1}{4}\frac{\pi}{\rho} D^2 d {B_O}^2 c v \tag{3.5}$$

Where

$$c = \frac{1}{2}\left[1 - \frac{1}{4}\frac{1}{\left(1+\frac{r}{R}\right)^2\left(\frac{R-r}{D}\right)^2}\right] \tag{3.6}$$

In the context of electromagnetic retarder brakes, the force applied for braking is determined, and the speed is expressed in its tangential representation. The calculation of various other parametric factors hinges on the specific characteristics of the electromagnetic retarder brake. Equations (3.4) and (3.5) are in full accordance with Smythe's findings, particularly in the low-speed domain.

Wouterse has observed a striking resemblance between the contemporary disc brake and a DC induction motor. The initial magnetic flux remains undisturbed despite a minor rotor current magnetic field generated by low rotor speed, resulting in a corresponding torque proportional to the velocity. The rotor system's current source is primarily influenced by its high-speed orientation, leading the initial primary flow to follow a leakage path that is perpendicular to the teeth. Wouterse's research has highlighted three significant occurrences within the air gap magnetic field at various velocities:

- The field is only slightly different at very low speeds from the field at nil velocity.
- The average induction underneath the pole is considerably less than Bo at the velocity at which the maximum drag force is exerted.

- The magnet induction at higher speeds appears to reduce further. Based on this assessment, in the high-speed region, Wouterse suggested:

$$F_e(v) = F_e \frac{2}{\frac{v_k}{v} + \frac{v}{v_k}} \tag{3.7}$$

With

$$\hat{F}_e = \frac{1}{\mu_o} \sqrt{\left(\left(\frac{c}{\xi}\right) \frac{\pi}{4} D^2 {B_o}^2\right) \sqrt{\left(\frac{x}{D}\right)}} \tag{3.8}$$

And

$$v_k = \frac{2}{\mu_o} \sqrt{\left(\frac{1}{c\xi}\right) \frac{\rho}{d}} \sqrt{\left(\frac{x}{D}\right)} \tag{3.9}$$

Where

ρ = disc material-specific resistance

d = thickness of disc

D = Soft iron poles diameter, D indicates a circle diameter with the same area as the poles ' face, for non-circular pole

ξ = Zone width ratio, in asymptotic current poles distribution, to the air gap

c = Proportionality variable, the proportion of total disc contour resistance (outer curve) to disc contour resistance (outer curve) part under pole

v = rotating disk tangential speed, evaluated at the pole center

v_k = Critical speed, i.e., maximum expanded force at the corresponding speed

B_o = zero speed air gap induction

x = Air gap between poles with disk thickness or coordinates perpendicular to the air gap

r = distance between the center of the disc and the center of the pole projection area

"In his proposal, Wouterse also incorporated a well-established high-speed principle, which posits that the drag force exhibits an inverse proportionality to the velocity, denoted as v^(-1). He subsequently modified the high-speed model to incorporate this characteristic explicitly.

As a result, the model closely aligns with the observed experimental outcomes within the high-speed domain."

3.3. Mathematical modeling of proposed electromagnetic retarder

The mathematical framework of the Electromagnetic retarder (EMR) articulates the braking torque concerning several key design variables, including the thickness of the braking disks, the electrical conductivity of the disks, and the distance of the air gap between the center of the disk and the center of the predicted region. Figure 3.1 illustrates the schematic depiction of the EMR.

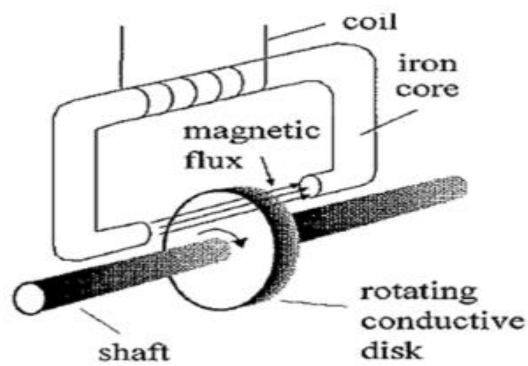

Figure 3.1. Schematic diagram of an EMR (Talaat, 2014)

Designate S as the pole area, R as the radius of the disk, r as the distance between the pole center and the center of the disk, and d as the thickness of the disk. The total flux, denoted as φ, circulating the iron core is expressed as follows (Karakoc et al., 2016):

$$\varphi = \frac{F}{R} \tag{3.10}$$

Where F and R denote MMF and reluctance, respectively.

$$F = Ni \tag{3.11}$$

$$R = \frac{l_g}{\mu_o S} \tag{3.12}$$

Where N, i, l_g and μ_o represent the respective quantities of the number of coil turns, current flowing through the electromagnet (EM) coil, air-gap length, and air permeability. Assuming an infinitely high permeability for the iron core, we can consider its reluctance negligible, effectively reducing the total reluctance to the air. Utilizing equations (3.10) through (3.12), the magnetic flux density can be determined as follows:

$$B = \frac{\varphi}{S} = \frac{1}{S}\frac{F}{R} = \frac{\mu_O N i}{l_g} \tag{3.13}$$

The density of the current which is induced at the pole center is given by

$$J = \sigma\left(R\dot{\theta} \times B\right) \tag{3.14}$$

Where σ indicates the disk's material's electrical conductivity and $\dot{\theta}$ represents the disk's angular velocity. Let Pd stand for the power that electromagnetic retarder dissipates. If we assume that all of this power is transformed into braking torque Tb, we may express braking torque as

$$T_b = \frac{P_d}{\dot{\theta}} \tag{3.15}$$

Using equation. (3.14) total power dissipation can be expressed as

$$P_d = \rho J^2 \times volume = \rho\sigma R^2 S d\dot{\theta}B^2 \tag{3.16}$$

Where ρ denotes the resistivity of the disk. Therefore, using Eqn. (3.15), braking torque can be expressed as

$$T_b = \rho\sigma R^2 S d\left(\frac{\mu_O N}{l_g}\right)^2 i^2\dot{\theta} \tag{3.17}$$

Equation (3.17) represents the proposed mathematical model of the electromagnetic retarder for Braking torque

Modeling of dc motor

$$T_e = K_e I_a \tag{3.18}$$

$$E = K_b\omega \tag{3.19}$$

$$V = E + I_a R_a + L\frac{dI_a}{dt} \tag{3.20}$$

Taking the Laplace Transform of equation (3.20)

$$V = E + I_a R_a + sLI_a\ ,\ \frac{(V-E)}{R_a + sL} = I_a \tag{3.21}$$

Equation (3.21) gives the expression of the armature current of the DC motor.

$$T_e = T_L + B\omega + J\frac{d\omega}{dt} \qquad (3.22)$$

Taking the Laplace Transform of equation (3.22)

$$T_e = T_L + B\omega + sJ\omega, \quad \frac{(T_e - T_L)}{B + sJ} = \omega \qquad (3.23)$$

Equation (3.23) expresses the angular speed of the DC motor.

Electromagnetic retarder braking torque functions as an applied load torque within the mathematical model of a DC motor. Consequently, when formulating the mathematical representation of the DC motor, substitute the load torque with the braking torque generated by the electromagnetic retarder (Pandey et al. 2015).

$$T_L = T_b$$

Where T_b represents the braking torque of the electromagnetic retarder.

$$\frac{(T_e - T_b)}{B + sJ} = \omega \qquad (3.23)$$

$$\frac{T_e - \left(\rho\sigma R^2 Sd\left(\frac{\mu_O N}{I_g}\right)^2 i^2 \dot{\theta}\right)}{B + sJ} = \omega \qquad (3.24)$$

Equation (3.24) represents the mathematical model of the electromagnetic retarder for the motor speed

Consider the case in which the DC motor rotates at a constant speed. Selecting angular speed as the output

$$J_m\frac{d\omega}{dt} + B\omega = T_e - T_L \qquad (3.25)$$

Where J is the moment of inertia and B is the frictional coefficient.

Using equations (3.18), (3.20) and (3.25), the dc motor dynamic equation can be written as

$$L\frac{dI_a}{dt} + R_a I_a + k_b\omega = V \qquad (3.26)$$

$$J\frac{d\omega}{dt} + B\omega - k_e I_a = -T_L \qquad (3.27)$$

Electrical Time Constant L/Ra is very small compared to the mechanical time constant J/B; therefore, it can be neglected. By neglecting the term dIa/dt, equation (3.26) becomes

$$I_a = \frac{1}{R_a}V - \frac{k_b}{R_a}\omega \tag{3.28}$$

Substituting equation (3.28) in equation (3.27) and assuming $k_b = k_e = k$, we get

$$\frac{d\omega}{dt} + \left(\frac{B}{J} + \frac{k^2}{JR_a}\right)\omega = -\frac{1}{J}T_L + \frac{k}{JR_a}V \tag{3.29}$$

Therefore, the motor will experience two external sources: the input voltage V to drive the motor and the load torque T_L.

State space modeling can also represent the mathematical model of the electromagnetic retarder.

Considering an angular velocity as the output. It can be expressed as

$$y = \omega \tag{3.30}$$

Considering equations (3.26) and (3.27) and selecting the state variables as $x_1 = i_a x_2 = \omega$ We obtain

$$R_a x_1 + L\dot{x}_1 + kx_2 = V \tag{3.31}$$

$$J\dot{x}_2 + Bx_2 - kx_1 = -T_L \tag{3.32}$$

Rearranging equations (3.31) and (3.32), we obtain state equations

$$\dot{x}_1 = -\frac{R_a}{L}x_1 - \frac{k}{L}x_2 + \frac{1}{L}V \tag{3.33}$$

$$\dot{x}_2 = \frac{k}{J}x_1 - \frac{B}{J}x_2 - \frac{1}{J}T_L \tag{3.34}$$

The output equation can be expressed as

$$y = x_2 \tag{3.35}$$

Therefore, the state space description can be expressed as

State equation $\dot{x} = Ax + Bu$ (3.36)

Output equation $y = cx$ (3.37)

Where the state vector is

$$x = \begin{bmatrix} x_1 \\ x_2 \end{bmatrix}$$

The input vector is

$$u = \begin{bmatrix} V \\ T_L \end{bmatrix}$$

Equation (3.38) gives the system matrices A and B.

System matrices are

$$A = \begin{bmatrix} \frac{-R_a}{L} & \frac{-k}{L} \\ \frac{k}{J} & \frac{-B}{J} \end{bmatrix} \quad , \quad B = \begin{bmatrix} \frac{1}{L} & 0 \\ 0 & \frac{-1}{J} \end{bmatrix} \text{ and } \quad c = [0 \quad 1] \qquad (3.38)$$

The visual representation in Figure 3.2 illustrates that the electromagnetic retarder braking torque functions as the load torque for the DC motor. Furthermore, the transfer functions for the components depicted in Figure 3.2 have been developed based on the mathematical model.

Where: V: input voltage (V), R_a: resistance of the armature (Ω), L_a: inductance of the armature (H), K_e: back EMF constant (V/rad/s) T_e: electromagnetic torque (kNm), B: viscous friction coefficient (Nms/rad), J: moment of inertia (kgm^2), Tb: braking torque (kNm), ω: rotational speed (rad/s).

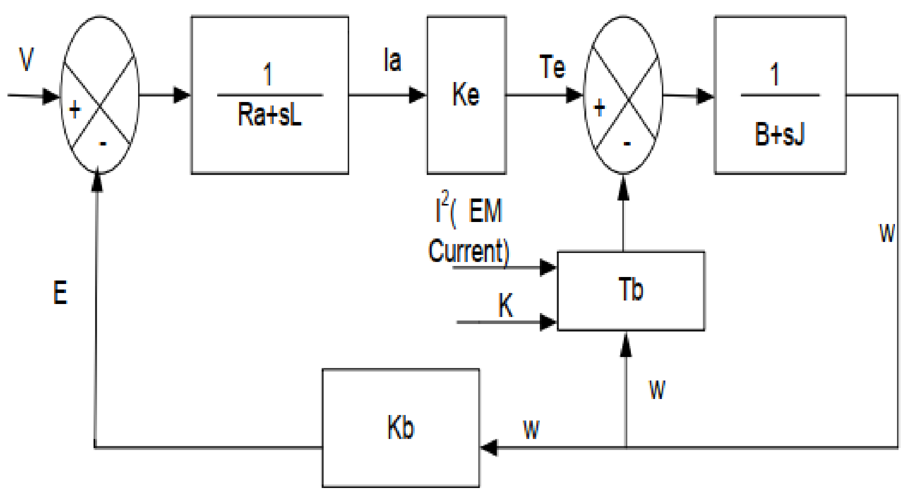

Figure 3.2. Block diagram representation of EMR mathematical model

4. RESULTS AND DISCUSSIONS

4.1. Introduction

Simulation offers a secure and cost-effective means for exploring various system models. This chapter delves into the electromagnetic retarder (EMR) simulation and elaborates on creating controllers by applying soft computing methodologies. Specifically, this involves using soft computing techniques like FLC and PSO for controller development.

4.2. Simulation of EMR Existing Control

Existing control involves manipulating the electromagnet current as the sole means of control. Adjusting the current in the electromagnet alters the degree of electromagnetic retarder induced in the disc, resulting in a variation in the generated electromagnetic retarder braking. Figure 4.1 illustrates the schematic representation of the system in the absence of electromagnetic retarder application, while Figure 4.2 portrays the system's block diagram following the application of electromagnetic retarder.

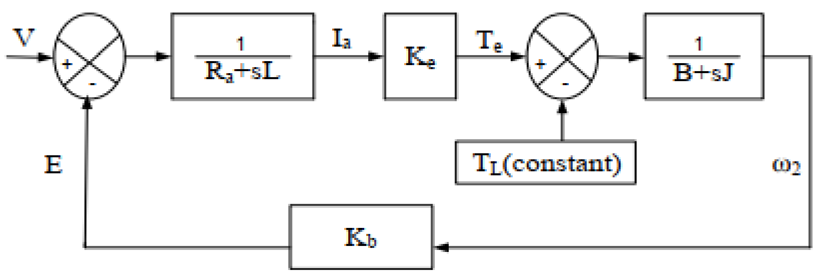

Figure 4. 1. System's block diagram without electromagnetic retarder

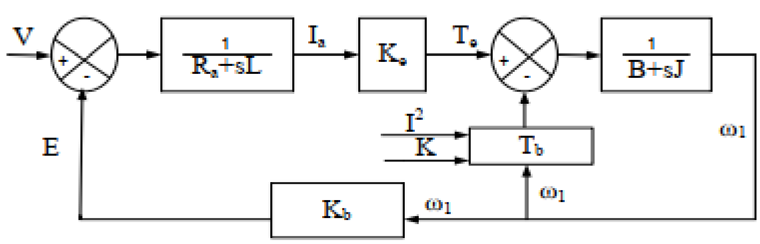

Figure 4. 2. System's block diagram with electromagnetic retarder

Figure 4.3 illustrates a notable reduction in motor speed, with the RPM decreased to 450 RPM without activating the EMR system.

With activating EMR the speed is reduced to 190RPM as shown figure 4.4, which is better than existing control but still controllers need to be employed to enhance the braking performance of the electromagnetic retarder (EMR). Figure 4.3 displays speed variations in the absence of EMR, Figure 4.4 depicts the speed fluctuations with EMR alone.

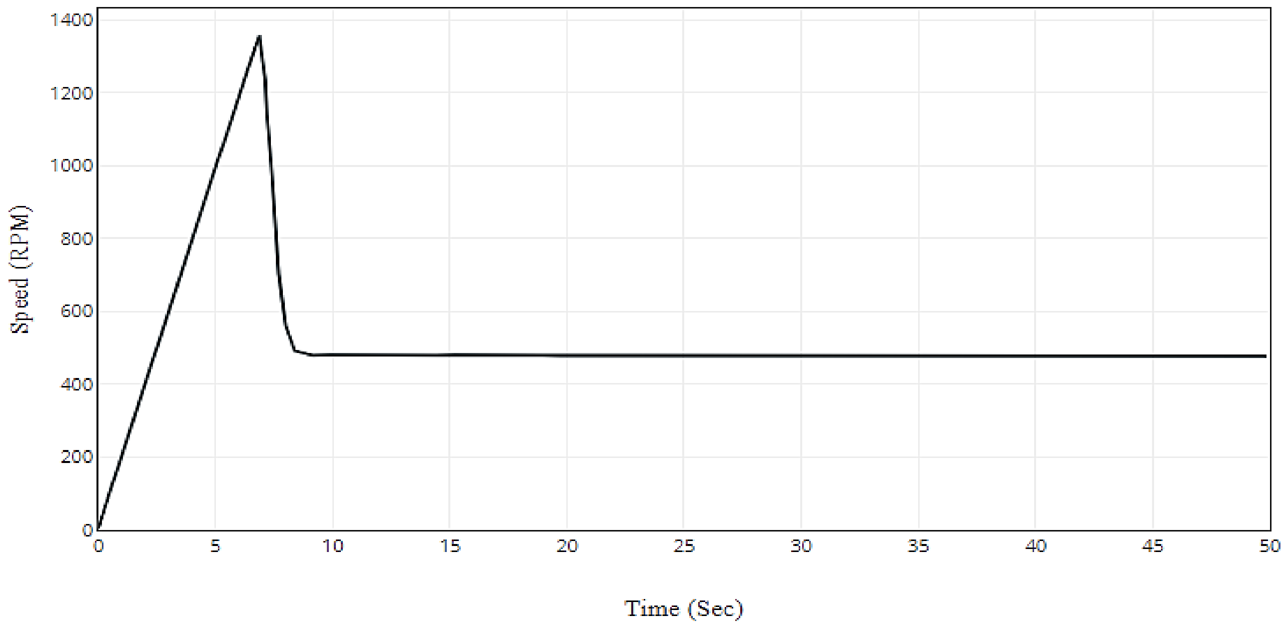

Figure 4. 3. Speed variation without electromagnetic retarder

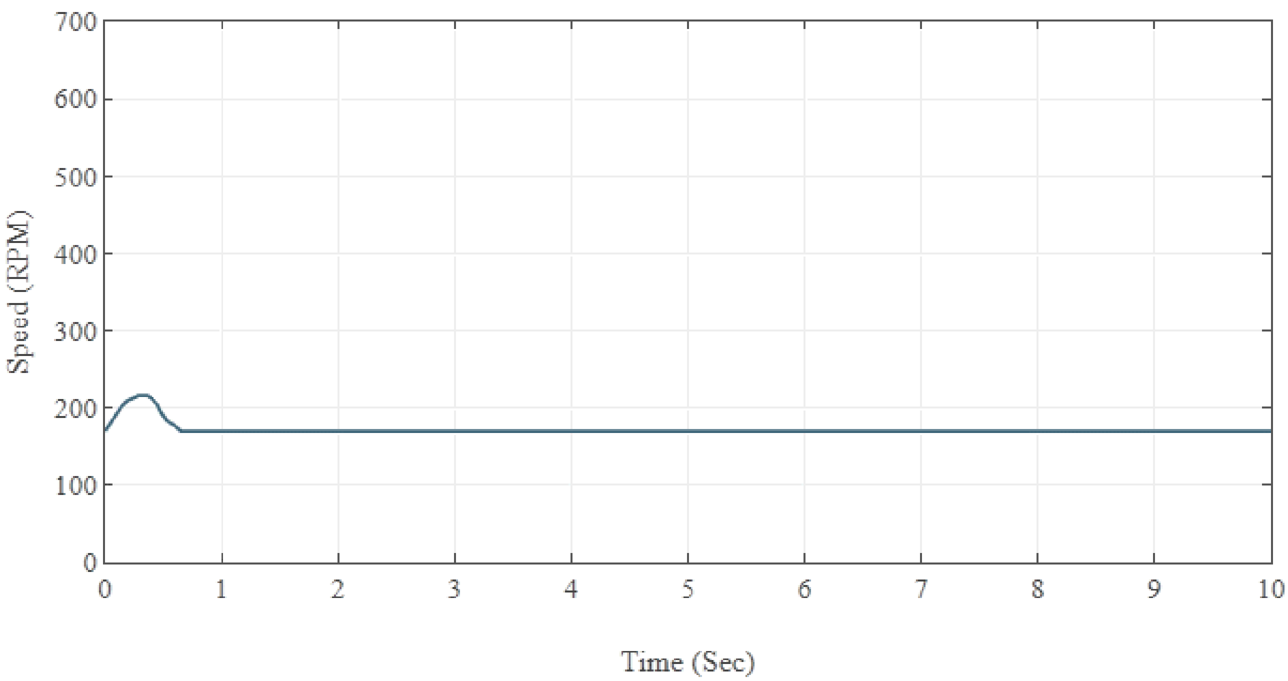

Figure 4. 4. Speed variation using electromagnetic retarder

4.3. Simulation of EMR Fuzzy logic controller

A fuzzy logic controller implements a fuzzy inference system, facilitating the development of linguistic-based control strategies that yield superior outcomes compared to existing control approaches. Fuzzy sets are mathematically crafted to represent levels of uncertainty and difficulty, offering a versatile tool to address imprecision in various contexts. In fuzzy logic, the transition from membership to non-membership occurs gradually, avoiding abrupt shifts. Fuzzy logic provides a means to model systems based on human-like intelligence, effectively handling challenges such as inaccuracy, vagueness, lack of specificity, and incompatibility. A fuzzy set encompasses a group of elements with unique membership function values within the range, and a single membership feature defines each fuzzy set entirely. Fuzzy membership functions can take various forms, including triangles, trapezoids, Gaussians, bells, and sigmoidal. The process of fuzzification is essential for converting crisp inputs into fuzzy ones. After the fuzzy control algorithm generates an output, the subsequent step, defuzzification, is necessary. A fuzzy logic control system comprises three key components: fuzzification, approximate reasoning, and defuzzification, as depicted in Figure 4.5 in the context of a fuzzy knowledge-based system(Hadziselimovic et al., 2008).

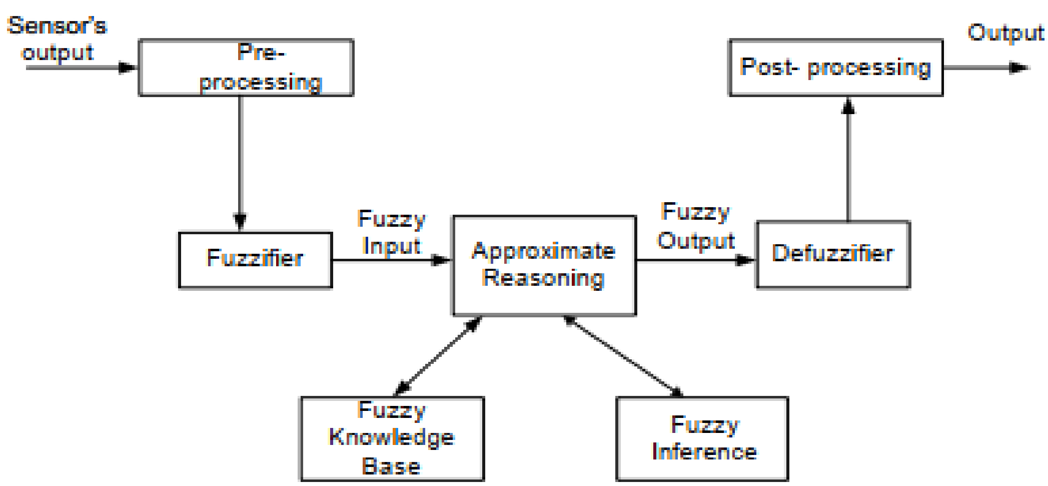

Figure 4. 5. Fuzzy knowledge-based system

The components depicted in Figure 4.5 can be elucidated as follows:

a) Preprocessing: In this stage, you can enter any desired information. Emphasizing its importance, it is imperative to employ Quill It for paraphrasing.

b) Fuzzification: This operation aligns the system with the fuzzy set representation of system state variables within the "antecedent" of rules, converting crisp input values into fuzzy output values.

c) Fuzzy Knowledge Base: This repository contains essential data about the application domain and control parameters. It encompasses the following elements:

   i) Fuzzy sets that elucidate the semantic meaning of linguistic values for system states and output variables.

   ii) Fuzzy rules are structured as "If x is A, then y is B," where x represents the state variable and y is the output variable. A and B are linguistic descriptors. The fundamental function of a fuzzy rule is to present a defined control policy through a set of rules for an experienced process operator.

d) Fuzzy Inference: The development of the inference engine in the fuzzy knowledge base involves two primary approaches: (1) composition-based inference and (2) individual rule-based inference, with the latter being the more common choice.

e) Defuzzification: This process converts fuzzy sets of values into crisp values.

f) Post-processing: After defuzzification, the performance of a fuzzy system in its physical domain undergoes de-normalization.

The fuzzy rule-based model can be categorized into two main types (Kado, 2009):

1. Mamdani Model: In the Mamdani model, both the system's input side (known as the antecedent part) and the output side (referred to as the consequence part) are characterized by fuzziness.
2. Takagi-Sugeno-Kang (TSK) Model: This model features fuzzy input pairs that establish a specific relationship with the output through a well-defined mapping. It combines elements of both fuzzy and no fuzzy models.

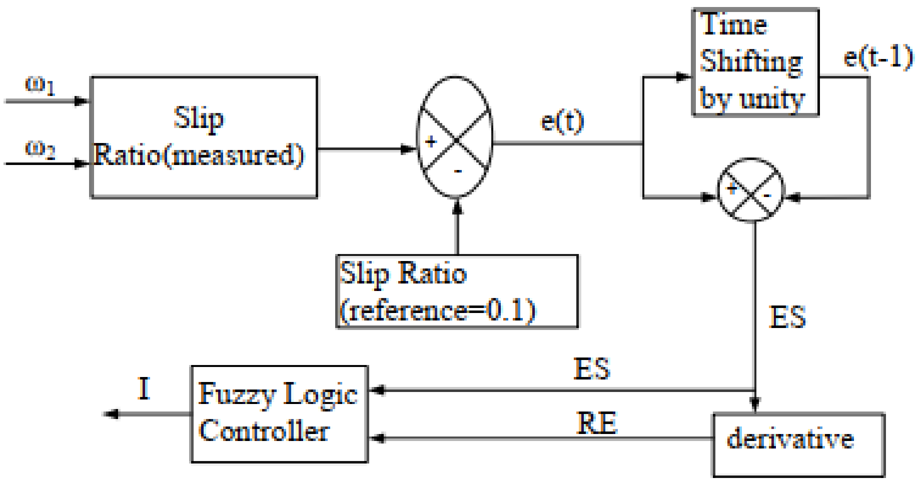

Figure 4. 6. Block diagram of fuzzy logic controller (FLC) designed for (EMR).

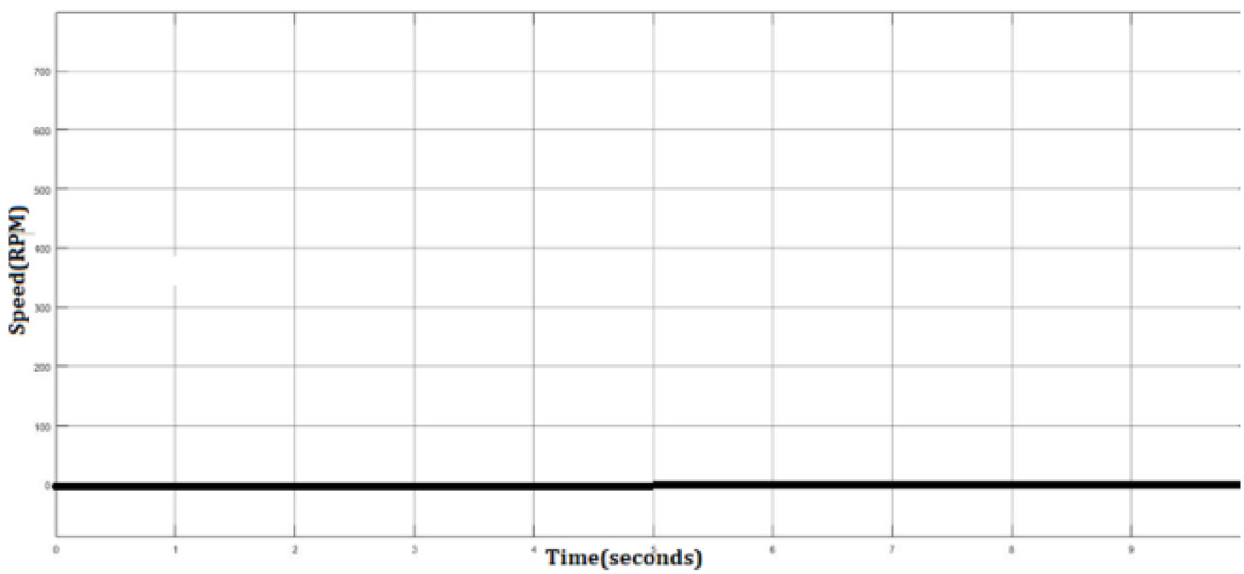

Figure 4. 7. Speed variation using electromagnetic retarder with FLC

A comprehensive system analysis is conducted, integrating EMR with Fuzzy Logic Controller (FLC). Figure 4.8, presents the schematic representation for the FLC employed for regulating the flowing current through the electromagnet (EM) within the context of the electromagnetic retarder (EMR). The resultant electromagnet current is represented as I_{EM}.

The utilization of the rule base was instrumental in developing the Fuzzy Logic Controller (FLC), which played a crucial role in regulating the current provided to the electromagnet (EM) system in alignment with specific demands. These demands were contingent upon the extent of braking needed and the speed at which such braking was required. By employing the principles mentioned earlier in conjunction with empirical data, a comprehensive fuzzy rule base is meticulously constructed, ultimately successfully attaining the targeted control objectives.

A two-input, one-output parameter fuzzy controller can be employed to enhance the operational efficiency of EMR. The slip ratio, denoted as SR, is a measure of the speed after braking (ω_1) relative to the speed before braking (ω_2) with a specified target value for the slip ratio set at 0.1.

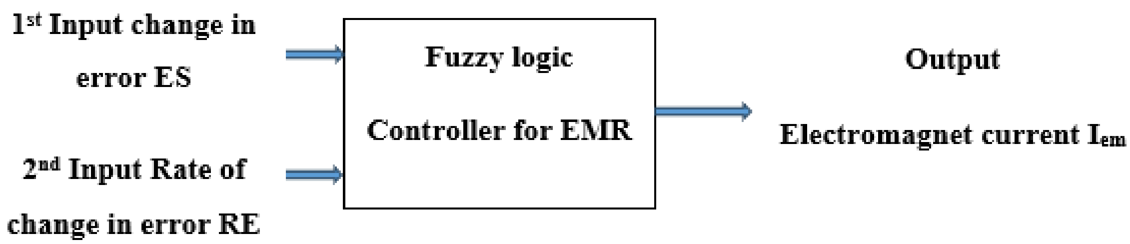

Figure 4. 8. Schematic representation for the FLC

From figure 4.1and 4.2, the slip ratio measured can be defined as

$$SR = {}^{\omega_1}/_{\omega_2} \tag{4.3}$$

The error e(t) given as;

e(t) = measured slip ratio - slip ratio sated (0.1)

The Change in error is taken as a first input parameter for the FLC and given by

$$ES = \Delta e(t) = e(t) - e(t-1) \tag{4.4}$$

The rate of change of error (RE) is a second input parameter and given by

$$RE = \frac{d(ES)}{dt} \tag{4.5}$$

The FLC output expressed by IU gives the electromagnet current (EM).

The universe of change in error (ES) was taken as [-3, 3], the universe of rate of change of error (RE) as [-3, 3] and the universe of EM current (IU) as [0, 6].

Using a rule base facilitated in Table 4.1 the creation of a fuzzy logic controller designed to regulate the current delivered to an electromagnetic retarder following specific demands. This regulation, in turn, hinges on the braking force required to minimize the slip ratio error. By employing the logic mentioned above a comprehensive fuzzy rule base is developed, culminating in attaining the desired level of control.

Table 4. 1. Fuzzy rule base matrix used for simulation

IU		Δe(t)						
		NB	NM	NS	ZS	PS	PM	PB
d(Δe(t))/dt	NB	NB	NB	NB	NB	NB	NB	NB
	NM	NB	NM	NM	NM	PS	PM	PB
	NS	NB	NM	NS	ZS	PS	PM	PB
	ZS	NB	NM	NS	ZS	PS	PM	PB
	PS	NB	NM	NS	ZS	PS	PM	PB
	PM	NB	PM	PM	PM	PM	PM	PB
	PB	NB	PB	PB	PB	PB	PB	PB

Table 4.1 illustrates the matrix of rules within the FLC, denoting the foundation of fuzzy rules. This matrix is structured as a 7x7 grid, necessitating the establishment of 49 distinct rules. Our analysis is centered on two input variables: prompting the adoption of seven membership functions with evenly spaced intervals. To enhance the precision of our outcomes, we've selected symmetrical triangular membership functions. To maintain uniformity in the triangle shapes among these seven membership functions, the apex of the triangular membership is anchored at 0, with an equal distribution on either side. As a result, the membership interval for these inputs is defined as [-3, 3], ensuring symmetry and balance in our approach.

In Table 4.1, the notation "NB" denotes the category of negative magnitude being large, "NM" signifies negative magnitude being of a moderate extent, "NS" designates negative magnitude being of a small scale, "ZS" represents a zero magnitude, "PS" corresponds to positive magnitude at a small level, "PM" denotes positive magnitude of moderate extent, and "PB" signifies positive magnitude on a significant scale.

The slip ratio reference value is assumed as 0.1.

From figure 4.3 and 4.4 $\omega_1 = 190, \omega_2 = 450$.

$$(SR)_{ref} = 0.1(assumed)$$

$$(SR)_{measured} = \frac{190}{450} = 0.42$$

The error can be given by

$$e(t) = (SR)_{measured} - (SR)_{ref}$$

$$e(t) = 0.42 - 0.1 = 0.32$$

If an error is shifted by unity, which gives time-shifting, it does not cause any change in magnitude of change in error.

$$\Delta e(t) = 0.32$$

The absolute value of $\Delta\, e(t)$ must be evenly apportioned among seven distinct membership functions, each receiving a share of $\frac{\Delta e(t)}{7} = 0.04$, resulting in a uniform distribution of 0.04 across each membership function. Tables 4.2 and 4.3 provide the specific range of membership functions for the initial change in error and the subsequent rate of change of error for the first and second input, respectively.

Table 4. 2. Range of membership functions for first input (change in error)

Membership Function	Range
NB	0-0.04
NM	0.04-0.08
NS	0.12-0.16
ZS	0.16-0.20
PS	0.20-0.24
PM	0.24-0.28
PB	0.28-0.32

The merit of employing this fuzzy controller stems from its inherent adaptability, enabling it to adjust the current input to the electromagnetic system automatically based on the specific braking demand. This results in decreased losses, enhanced precision in control, increased efficiency, and swifter and more accurate response times.

Table 4. 3. Range of membership functions for second input (rate of change of error)

Membership Function	Range
NB	0-0.03
NM	0.03-0.06
NS	0.06-0.09
ZS	0.09-0.12
PS	0.12-0.15
PM	0.15-0.18
PB	0.18-0.24

Figure 4.9 depicts the constructed Fuzzy Inference System (FIS) for the Electromagnetic retarder (EMR). Furthermore, Figures 4.10, 4.11, and 4.12 illustrate the membership functions corresponding to first input, second input, and the output within the designed EMR FIS, respectively.

In Figure 4.13, we can observe the rule editor of the FIS, while Figure 4.14 provides a view of the rule viewer specific to the designed FIS. Furthermore, Figure 4.15 displays a surface plot with first input plotted on the x-axis, second input on the y-axis, and output on the z-axis. This three-dimensional representation on the surface plot illustrates how changes in either or both inputs affect the output, effectively mapping the relationship. Developing a fuzzy logic controller involves the utilization of a Mamdani-type FIS with two inputs and one output. Triangular membership functions have been applied to both the input and output components.

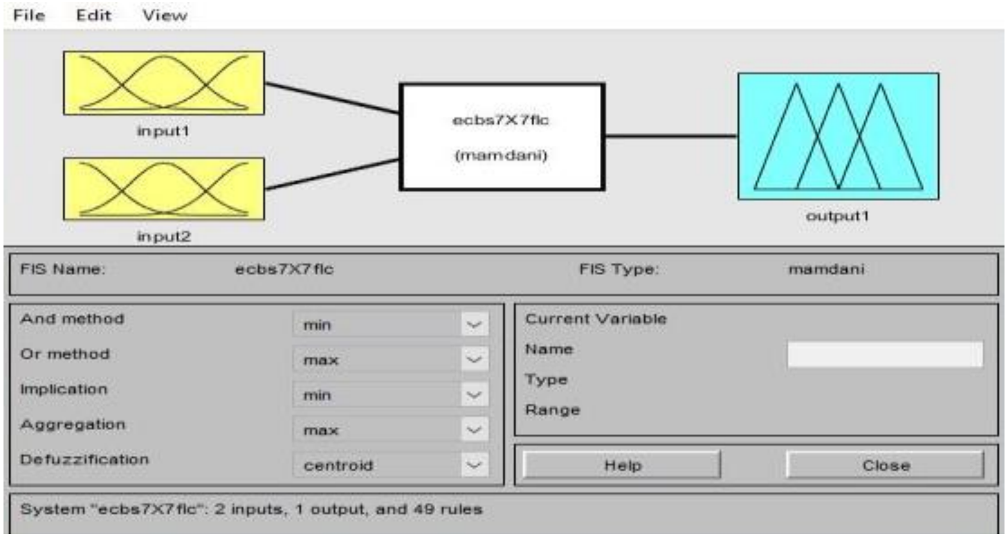

Figure 4. 9. The fuzzy inference system of EMR used for simulation

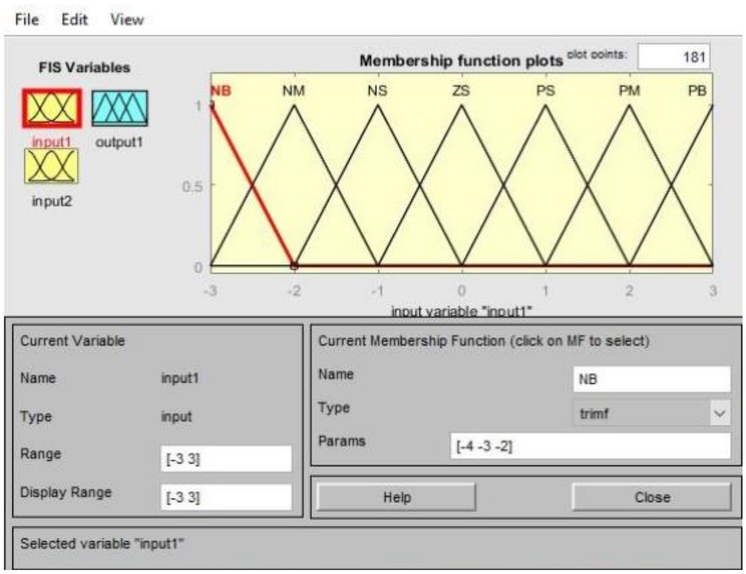

Figure 4. 10. Membership function for first input (change in error) of EMR FIS used for simulation

Figure 4.10 illustrates the relationship between error change (ES) and first input, characterized by seven distinct membership functions. These functions are denoted as follows: NB (Negative Big), NM (Negative Medium), NS (Negative Small), ZS (Zero Small), PS (Positive Small), and PB (Positive Big). The range of these membership functions is as follows: NB ranges from -4 to -2, NM from -3 to -1, NS from -2 to 0, ZS from -1 to 1, PS from 0 to 2, PM from 1 to 3, and PB from 2 to 4. It's important to note that a triangular-type membership function has been selected for this representation.

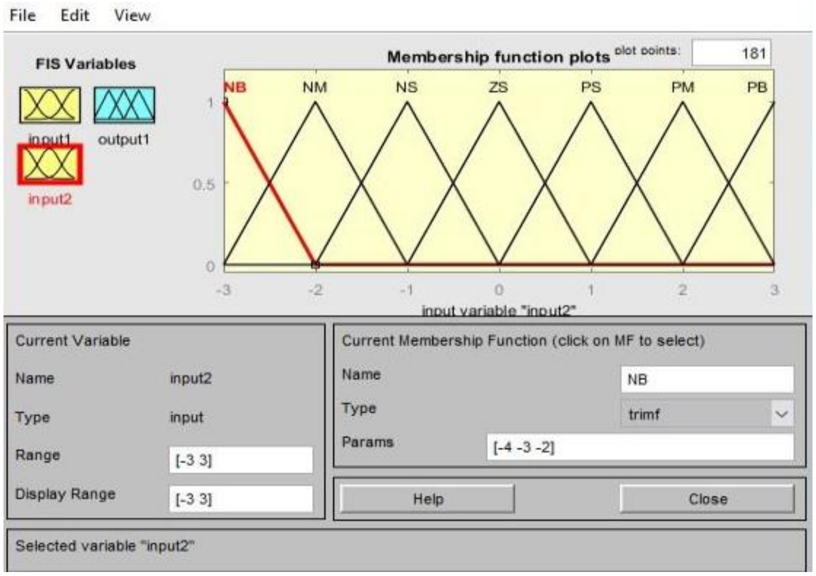

Figure 4. 11. Membership function for second input (rate of change of error) of EMR FIS used for simulation

In Figure 4.11, we present the membership functions for second input, which signifies the rate of change in error (RE). Seven distinct membership functions are employed to characterize this input. The range of values covered by these membership functions is as follows: NB ranges from -4 to -2, NM from -3 to -1, NS from -2 to 0, ZS from -1 to 1, PS from 0 to 2, PM from 1 to 3, and PB from 2 to 4. These membership functions take on a triangular shape.

It's worth noting that the same number and type of membership functions represent the output, as depicted in Figure 4.9. For the output, the ranges for NB, NM, NS, ZS, PS, PM, and PB are as follows: NB ranges from -1 to 1, NM from 0 to 2, NS from 1 to 3, ZS from 2 to 4, PS from 3 to 5, PM from 4 to 6, and PB from 5 to 7.

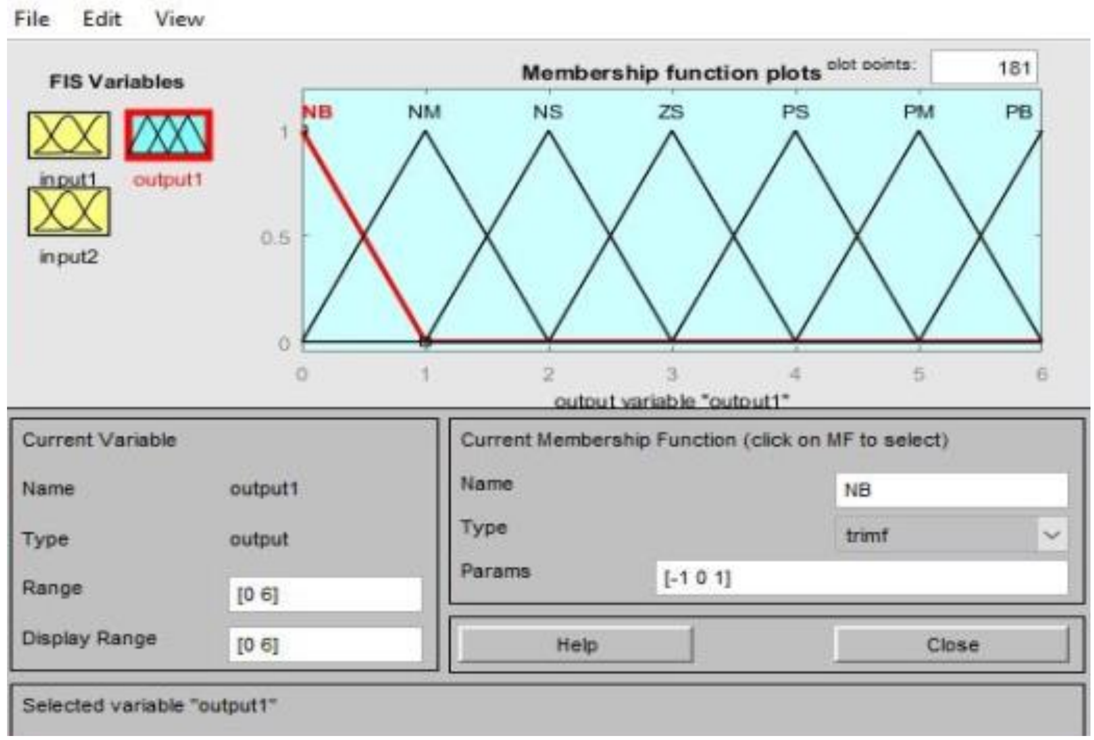

Figure 4. 12. Membership function for the output of EMR FIS used for simulation

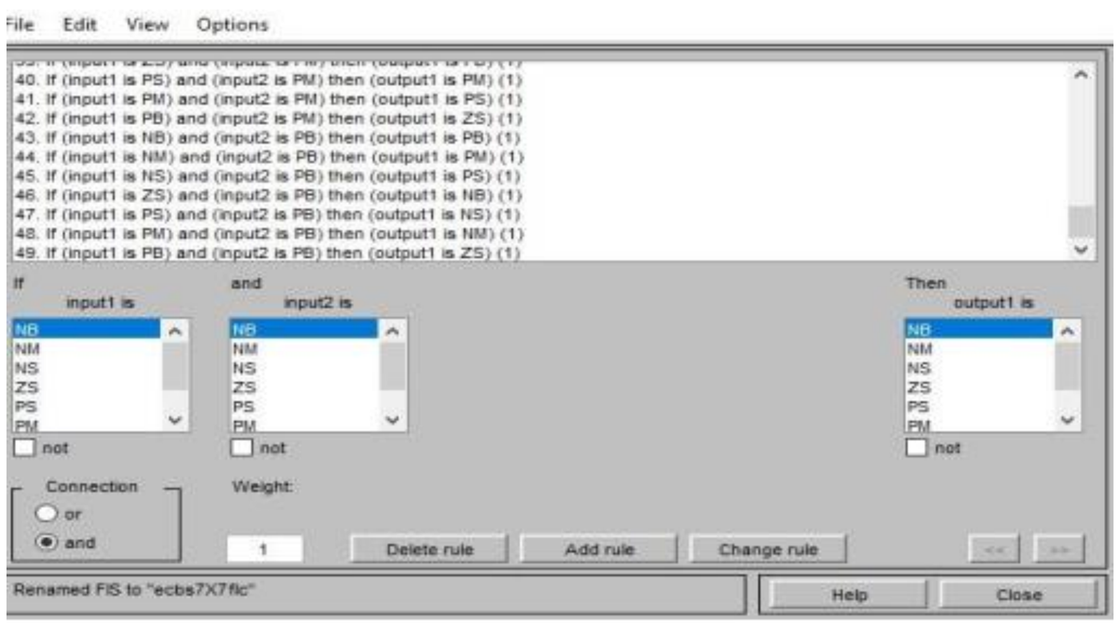

Figure 4. 13. Rule editor for the designed FIS used for simulation

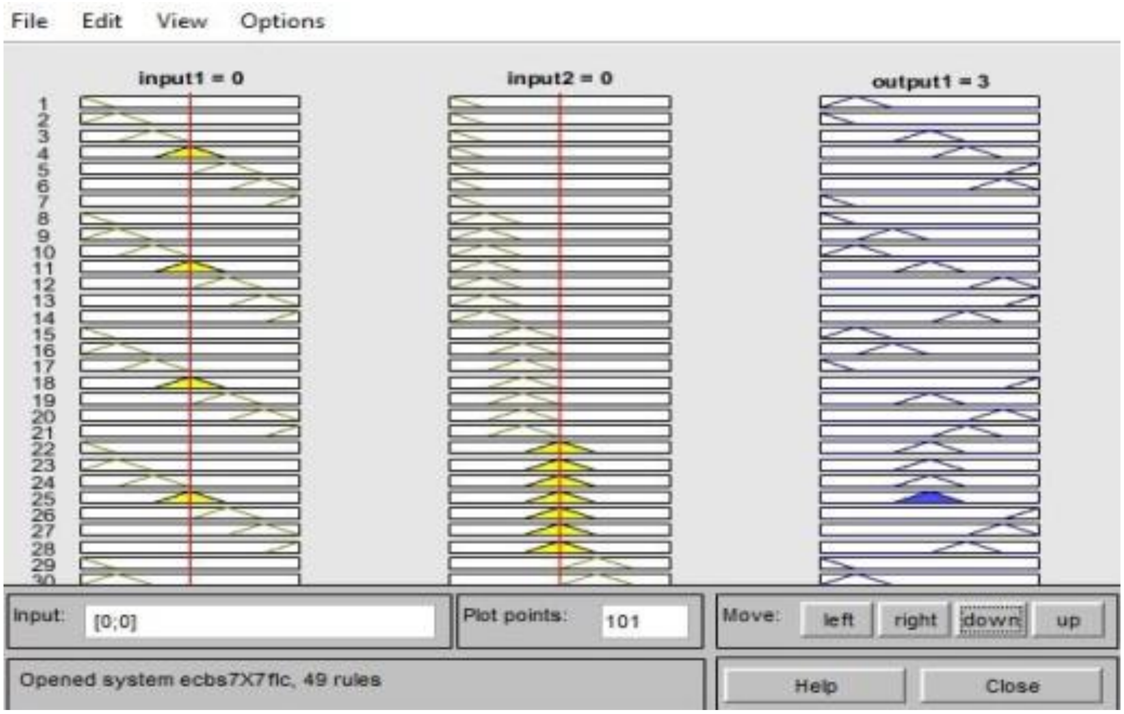

Figure 4. 14. Rule viewer for the designed fuzzy inference system used for simulation

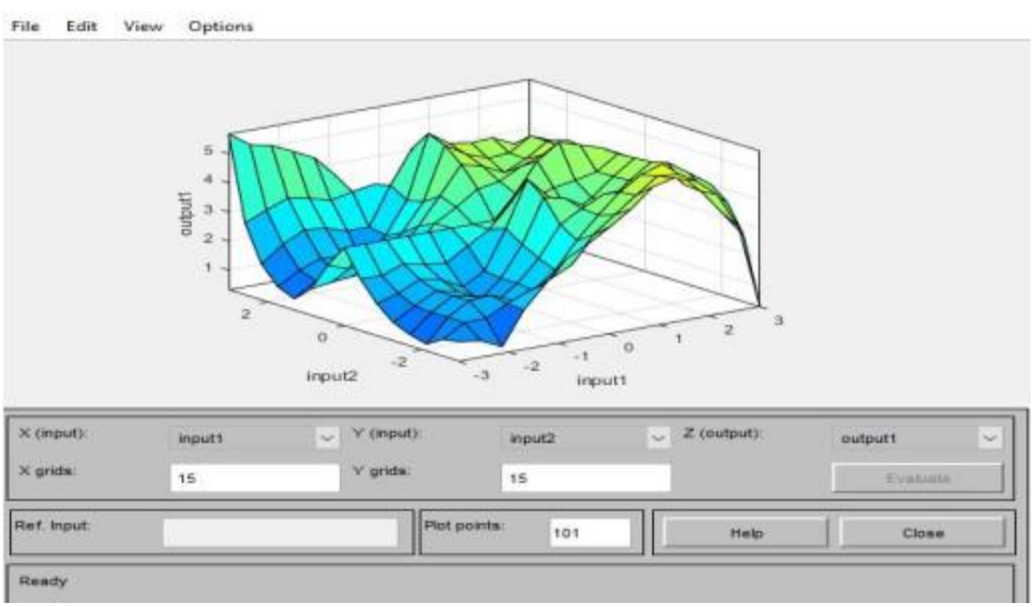

Figure 4. 15. Surface plot of the designed FIS

4.4. Simulation of EMR Particle Swarm Optimization (PSO) Controller

The primary aim PSO is to address computationally challenging optimization problems. It is technique that leverages swarm behavior and intelligent optimization principles. This approach has demonstrated its effectiveness across various domains requiring search and optimization solutions. PSO draws inspiration from natural phenomena, such as the collective behavior of birds and fish. Developed in 1995 by James Kennedy and Russ Eberhart, this technology employs many particles, simulating electron-like entities, which navigate a defined search space to locate a global optimum. These particles engage in immediate or partial communication with each other during their quest. Each iteration for every particle in PSO revolves around three key components: the best previous velocity and the best previous position within its neighborhood.

The PSO (Particle Swarm Optimization) algorithm ranks among the most widely employed artificial intelligence algorithms, drawing a direct parallel between biological behaviors and everyday engineering practices. It emulates the foraging nature of insects as they seek sustenance collectively, with each particle or insect perpetually questing for a predefined target while transmitting vital information to others in the swarm. Within this search space, particles operate with two key parameters: velocity and position. Through mutual communication, particles share knowledge about favorable positions and adapt their speeds and positions based on this information. It is essential to determine the fitness criteria and population size beforehand, directly dictating the number of particles. The initial quantity of particles is determined in line with the design specifications, and a specific number of iterations is chosen, continuing until the convergence criterion is met. The core principle of PSO revolves around propelling each particle towards its historically optimal position, known as the self-best position (P_{best}), and the best position achieved thus far by any particle in the swarm, referred to as the global best position (G_{best}). These advancements are orchestrated through equations (4.7) and (4.8). In every iteration, the algorithm identifies the best local positions (P_{best}) and, among these local candidates, determines the best position leading to the global optimum (G_{best}). In equations (4.7) and (4.8), we need to choose randomly the coefficient of acceleration and inertial weight according to the objective function's fitness level. The velocity of particle j in i^{th} iteration is given by equation (4.7). Position of j^{th} particle in the iteration is given by equation (4.8). This relation between the position and velocity of a particle can be expressed as

$$V_j(i) = V_j(i-1) + c_1 r_1 \left[p_{best.j} - X_j(i-1)\right] + c_2 r_2 \left[G_{best.j} - X_j(i-1)\right] \tag{4.7}$$

$$X_j(i) = X_j(i-1) + V_j(i) \tag{4.8}$$

Where

G_{best} = Global best position.

P_{best} = Self best position.

c_1 and c_2 = Acceleration coefficients.

r_1 and r_2 = Random numbers

$V_j(i)$ = Velocity of j^{th} particle in i^{th} iteration

$X_j(i)$ = Position of j^{th} particle in i^{th} iteration

It is imperative to verify the convergence of the present solution. The adopted approach is successful when all particle positions converge to a uniform set of values. If the convergence criteria are not satisfied, the procedure is reiterated, with the iteration number being updated as I = i + 1, and the new values for P (best, j) and G_{best} recalculated. This iterative process persists until all particles converge to the same optimal solution. The new X_j will be assessed after the new calculation. If fitness at X j is higher than P_{best}, then P_{best} = X_j and, fitness (P_{best}) = fitness (X_j), and (G_{best}) fitness = better fitness (P_{bes}t) at the last of the iteration.

An appropriately chosen inertia weight strikes a harmonious equilibrium between delving into global and local exploration, reducing the average number of iterations needed to attain the optimal solution. The determination of the inertia weight, denoted as 'W,' is established through the following equation:

$$W = W_{max} - \frac{W_{max} - W_{min}}{iter_{max}} \times iter \tag{4.9}$$

Where $iter_{max}$ is the maximum number of iterations (generations), and *iter* is the current number of iterations

From the equation of braking torque, T_b is given by

$$T_b = Ki^2\omega \tag{4.10}$$

The PSO technique is employed individually to optimize braking torque with current and speed. The algorithm, depicted in Figure 4.16, is shared for speed and current optimization processes.

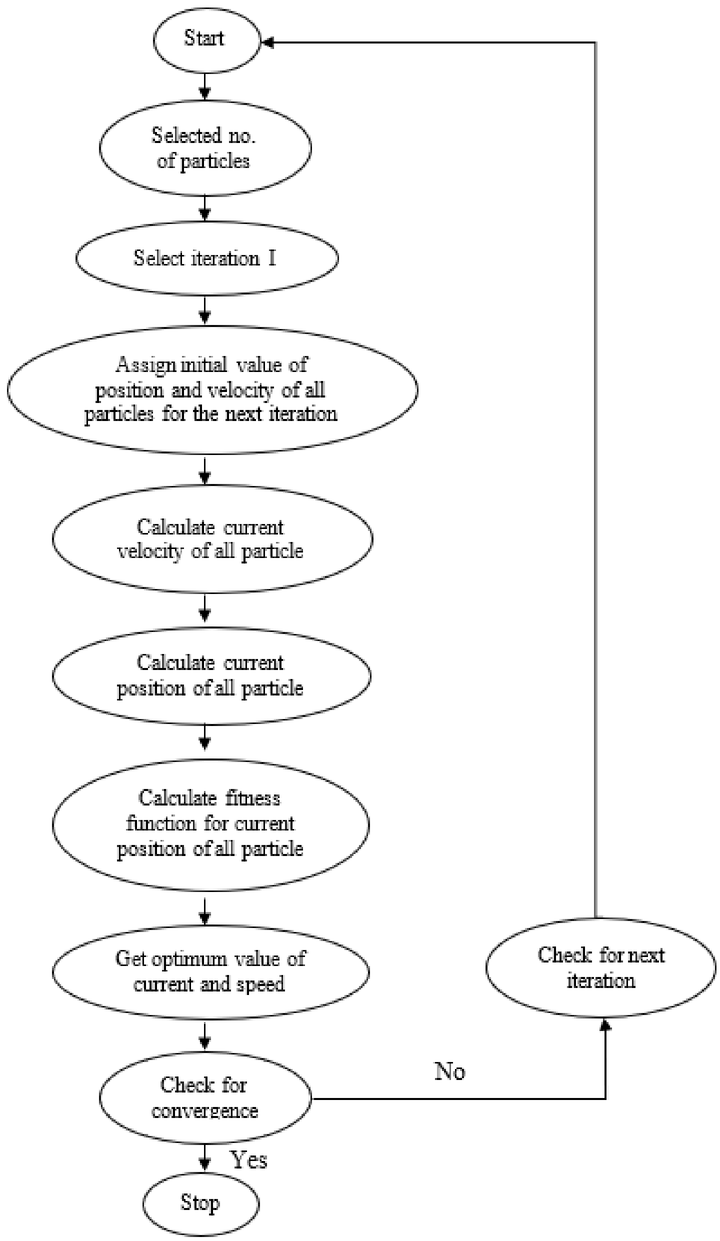

Figure 4. 16. Flowchart representation of PSO

4.4.1. Algorithm of Speed

Let the population size be five particles with the initial value assigned as ${\omega_1}^i = 560, {\omega_2}^i = 660, {\omega_3}^i = 790, {\omega_4}^i = 900, {\omega_5}^i = 980$.

The algorithm illustrated in the flowchart depicted in Figure 4.16 determined that the motor's speed, both with and without the application of electromagnetic retarder braking, ultimately converged during the 20th iteration.

4.4.2. Algorithm of Current

Let the size of the population be 5 particles with the initial value assigned as ${I_1}^i = 6.2, {I_2}^i = 6.7, {I_3}^i = 7.2, {I_4}^i = 8.2, {I_5}^i = 9$.

By employing the algorithm depicted in the flow chart of Figure 4.16, it was determined that the current of an electromagnet, both with and without the application of electromagnetic retarder braking, reaches a convergence point during the 20th iteration.

A comparison of a FLC and PSO techniques was employed to compare the precision of the EMR performance. Before braking, the motor operated at 1350 RPM. However, using the EMR braking resulted in a speed reduction to 450 RPM, which did not meet the desired specifications, as illustrated in Figures 4.4 and 4.5. The target speed reduction is achieved using PSO based EMR than FLC based EMR as depicted in Figure 4.17.

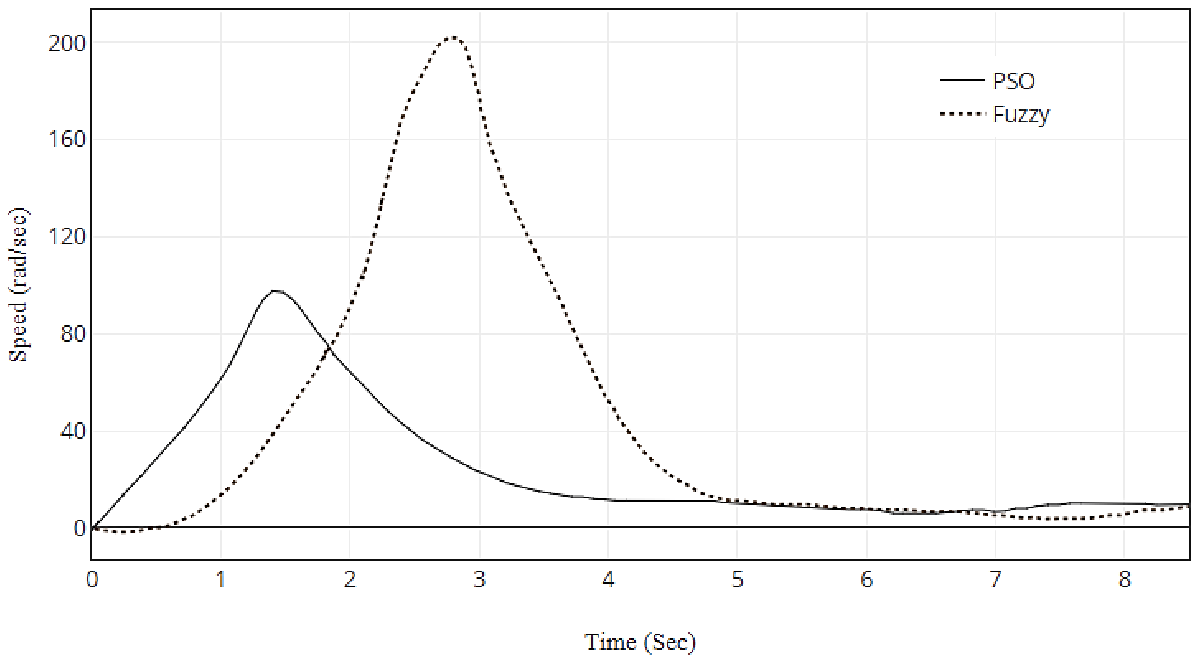

Figure 4. 17. Speed variation of electromagnetic retarder with FLC and PSO

Analysis of braking torque for initial iteration, and 20th iteration are shown in table 4.4, and 4.5. The remaining iterations are shown in Appendix A.

Table 4. 4. Analysis of braking torque for the initial iteration

S. No.	Current(A)	Speed (RPM)	Braking torque (KNm)
1	6.2	560	77
2	6.7	660	78.5
3	7.2	790	89.5
4	8.2	900	91.68
5	9	980	99.5

Table 4. 5. Analysis of braking torque for the 20th iteration

S. No.	Current(A)	Speed (RPM)	Braking torque(KNm)
1	9.1	972	99.5
2	8.9	971	99.6
3	9.0	970	98.78
4	9.0	971	99.1
5	9.0	970	98.99

Observing the relation between fitness value and iterations in a PSO algorithm exposes the search process as shown in figure 4.18. The x-axis indicates the number of iterations, while the y-axis shows the fitness value. Lower values for fitness typically indicate better solutions based on the problem's objective function.

The graph depicts a convergence curve, which shows how the average fitness value of the entire swarm changes over iterations. An ideal scenario shows a constant decline in fitness, indicating that the swarm is collectively focusing in on the best solution.

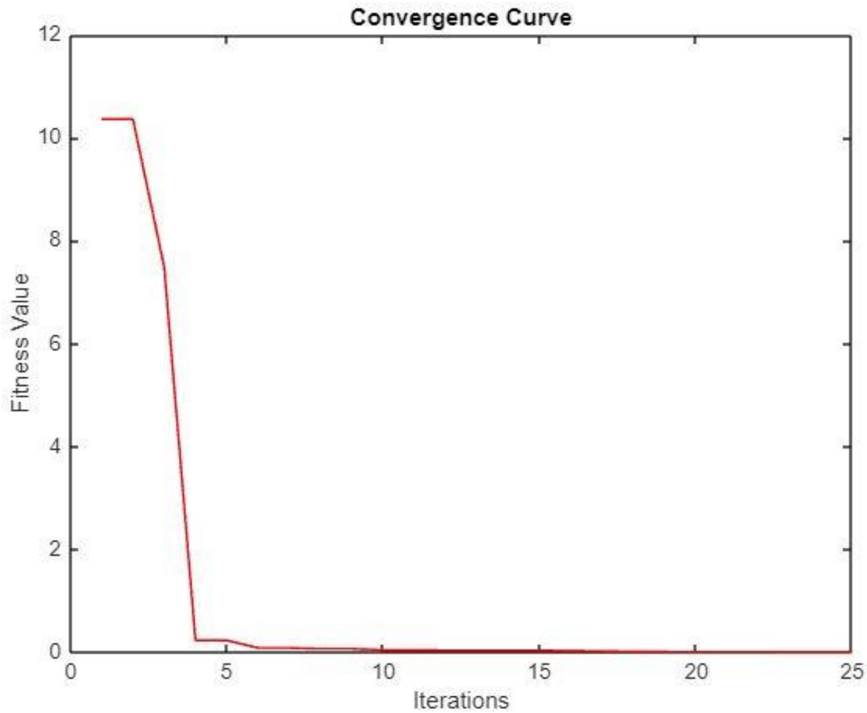

Figure 4. 18: Convergence curve of PSO

This decrease reflects the PSO's ability to find increasingly better solutions as the search progresses. Overall, the declining trend indicates that the PSO algorithm is convergent to a solution with a decent fitness value.

Table 4. 6. Comparison of settling time

S. No.	Motor speed	Settling time of FLC (Seconds)	Settling time of PSO (Seconds)
1	With EMR	7.5	3.5

Table 4. 7. Comparison of peak overshoot

S. No.	Motor speed	Peak overshoot of FLC (%)	Peak overshoot of PSO (%)
1	With EMR	30	12

The result shows that PSO gives the required result after 25 iterations at a faster rate when compared to FLC. It shows that PSO has better control dynamics than fuzzy logic controller with a smaller peak overshoot.

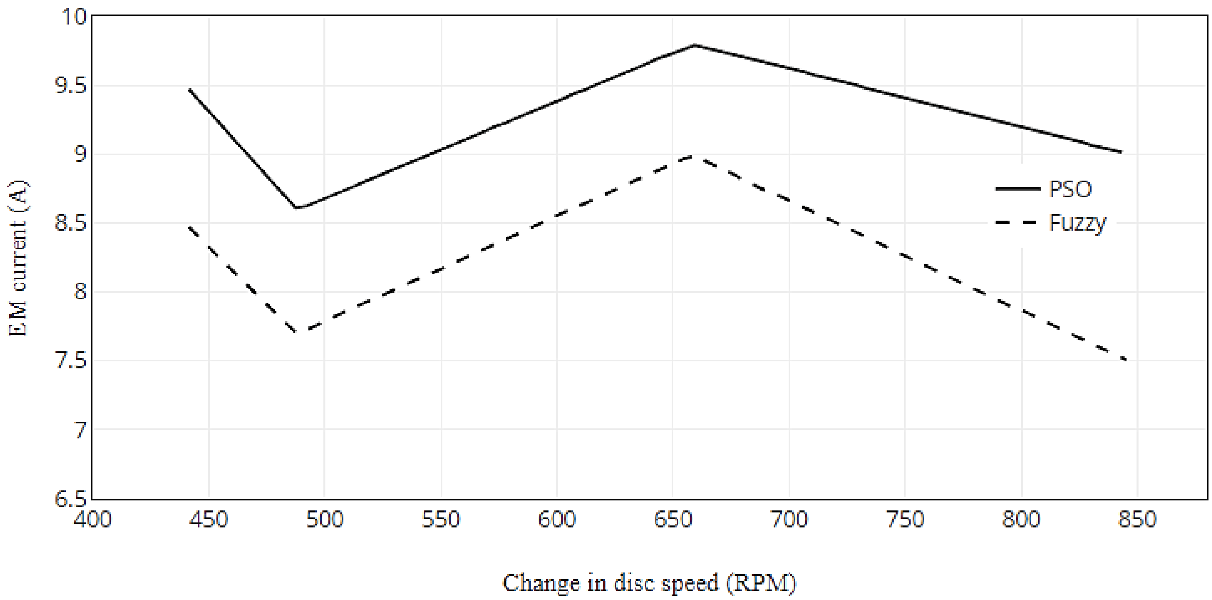

Figure 4. 19. Comparative plot showing EM current variation with change in disc speed for FLC and PSO

In Figure 4.19, a comparative analysis between FLC and PSO controllers is presented and The data illustrates that, for the same speed change value, the PSO controller-based EMR demonstrates the highest EM current and, consequently, the greatest braking torque, resulting in superior braking performance. Additionally, the PSO controller-based EMR exhibits the most favorable dynamic performance regarding settling time.

5. CONCLUSIONS AND RECOMMENDATIONS

5.1. Summary and Key Findings

The modelling and simulation of the electromagnetic retarder braking system was executed using MATLAB software. A simulation model of the DC motor was crafted, and the impact of electromagnetic retarder braking was treated as a negative load torque applied to the motor. Soft computing techniques, namely FLC and PSO, were employed to develop controllers for the EMR and subsequent simulation. The results indicated that the EMR with the PSO-based controller settled more rapidly with 3.5s than the EMR with a fuzzy logic controller of 7.5s, showcasing a lower peak overshoot value of 12% compared to the 30% peak overshoot value of FLC.

The simulation of a FLC applied to EMR, a 7x7 fuzzy inference system comprising 49 rules was meticulously designed. This system utilized two inputs, one for error change and the other for the error change rate, with the output representing electromagnet current. A Mamdani-type fuzzy inference system was employed, employing triangular membership functions for both input and output variables.

5.2. Conclusions

This study entailed the evaluation of a mathematical model and a software simulation representation of the electromagnetic retarder braking system, with a keen focus on assessing its performance. The electromagnetic retarder system involved a comprehensive exploration encompassing modeling and simulation harnessing the capabilities of controllers.

The emulation of the electromagnetic retarder was executed using fuzzy logic and particle swarm optimization. These intelligent control techniques were employed with the overarching objective of enhancing the system's overall braking performance.

The outcomes of this study were significant, as the application of soft computing-based controllers yielded a substantial improvement in the braking efficiency of the electromagnetic retarder. This breakthrough showcases the potential for soft computing techniques to advance electromagnetic retarder braking technology, offering promising prospects for safer and more efficient braking systems.

5.3. Recommendations for future work

To enhance both the performance and controllability of the electromagnetic retarder (EMR) a realm of other intelligent techniques may be harnessed to optimize the functionality of the EMR further. Moreover, it is possible to design a neuro-controller to govern and fine-tune the various parameters within the EMR, thereby enhancing its overall efficiency and adaptability. The integration of Electromagnetic retarder (EMR) with regenerative and anti-lock braking system should be a future research area to optimize the performance and efficiency of electromagnetic retarder. This research aims to pave the way for a comprehensive understanding and improvement of EMR.

REFERENCES

Busher, V., & Horoshko, V. (2019). Dual Electromagnetic Retarder Control System for Tuning Internal Combustion Engines. *Proceedings of the International Conference on Modern Electrical and Energy Systems, MEES 2019*, 26–29. https://doi.org/10.1109/MEES.2019.8896526

Enokizono, M., Todaka, T., & Takahashi, H. (2001). Electromagnetic retarder design using finite element analysis. *International Journal of Applied Electromagnetics and Mechanics*, *14*(1-4 SPEC.), 43–46. https://doi.org/10.3233/jae-2002-354

Aguiar, P. M., Jacquinot, J. F., & Sakellariou, D. (2009). Experimental and numerical examination of eddy (Foucault) currents in rotating micro-coils: Generation of heat and its impact on sample temperature. *Journal of Magnetic Resonance*, *200*(1), 6–14. https://doi.org/10.1016/j.jmr.2009.05.010

Albertz, D., Dappen, S., & Henneberger, G. (1996a). Calculation of the 3d non-linear eddy current field in moving conductors and its application to braking systems. *IEEE Transactions on Magnetics*, *32*(3 PART 2), 768–771. https://doi.org/10.1109/20.497353

Albertz, D., Dappen, S., & Henneberger, G. (1996b). Calculation of the 3D nonlinear eddy current field in moving conductors and its application to braking systems. *IEEE Transactions on Magnetics*, *32*(3), 768–771. https://doi.org/10.1109/20.497353

Chengye, L., & Jianming, S. (2013). Design technologies of eddy current retarder used in an automobile. *Applied Mechanics and Materials*, *251*, 134–138. https://doi.org/10.4028/www.scientific.net/AMM.251.134

Kimbrough, S. (2018). *SA E TECHNICAL Optimal Control of Electromagnetic Brake Retarders*. *41 2*.

Gay, S., & Ehsani, M. (2006). Parametric analysis of eddy-current brake performance by 3-D finite-element analysis. *Magnetics, IEEE Transactions On*, *42*, 319–328. https://doi.org/10.1109/TMAG.2005.860782

Gholizad, H., Funieru, B., & Binder, A. (2009). Direct Modeling of Motional Eddy Currents in Highly Saturated Solid Conductors by the Magnetic Equivalent Circuit Method. *IEEE Transactions on Magnetics*, *45*(3), 1016–1019. https://doi.org/10.1109/TMAG.2009.2012546

Ha, K.-H., Hong, J. P., Kim, G.-T., Lee, ju, & Kang, D. (1999). Study on the design for touch free linear eddy current brake. *Magnetics, IEEE Transactions On*, *35*, 4031–4033. https://doi.org/10.1109/20.800745

Routh, P. K., Sagar, P., Kumar, R., & Paul, S. (2008). Electromagnetic Braking System. *International Research Journal of Engineering and Technology*, *5744*(1), 97–100. www.irjet.net

Hadziselimovic, M., Virtic, P., Stumberger, G., Marcic, T., & Štumberger, B. (2008). Determining force characteristics of an electromagnetic brake using co-energy. *Journal of Magnetism and Magnetic Materials - J MAGN MAGN MATER*, *320*. https://doi.org/10.1016/j.jmmm.2008.04.013

He, R., Liu, X., & Liu, C. (2013). Brake Performance Analysis of ABS for Eddy Current and Electrohydraulic Hybrid Brake System. *Mathematical Problems in Engineering*, *2013*, 979384. https://doi.org/10.1155/2013/979384

Ihm, H.-B., Lee, S., Ham, S.-H., & Lee, ju. (2008). The influence of slit construction on the eddy current braking torque considered by 3D FEM analysis. *Proceedings of the 11th International Conference on Electrical Machines and Systems, ICEMS 2008*.

Kado, A. M. (2009). Analysis of The Harmonic Order Affecting The Eddy Current Braking Force in Electrical Machines. *Tikrit Journal of Engineering Sciences*, *16*(1 SE-Articles), 93–104. https://doi.org/10.25130/tjes.16.1.07

Karakoc, K., Suleman, A., & Park, E. J. (2016). Analytical modeling of eddy current brakes with the application of time varying magnetic fields. *Applied Mathematical Modelling*, *40*(2), 1168–1179.

Kou, B., Jin, Y., Zhang, H., & Zhang, L. (2014). Analysis and Design of Hybrid Excitation Linear Eddy Current Brake. *Energy Conversion, IEEE Transactions On*, *29*, 496–506. https://doi.org/10.1109/TEC.2014.2307164

Lee, K., & Park, K. (1999). Optimal robust control of a contactless brake system using an eddy current. *Mechatronics*, *9*(6), 615–631. https://doi.org/https://doi.org/10.1016/S0957-4158(99)00008-2

LEE, T. Y. K. and S. H. (2012). Combustion and Emission Characteristics of Wood Pyrolysis Oil-Butanol Blended Fuels in a Di Diesel Engine. *International Journal of …*, *13*(2), 293–300. https://doi.org/10.1007/s12239

LIU, C. (2008). Numerical analysis and experiment of unsteady thermal field of rotor plate for eddy current retarder. *Chinese Journal of Mechanical Engineering - CHIN J MECH ENG*, *21*. https://doi.org/10.3901/CJME.2008.04.071

Liu, C., Jiang, K., & Zhang, Y. (2011). Design and use of an eddy current retarder in an automobile. *International Journal of Automotive Technology*, *12*, 611–616. https://doi.org/10.1007/s12239-011-0071-3

Lubin, T., & Rezzoug, A. (2017). Improved 3-D Analytical Model for Axial-Flux Eddy-Current Couplings With Curvature Effects. *IEEE Transactions on Magnetics*, *PP*. https://doi.org/10.1109/TMAG.2017.2714628

Niu, B., Wang, D., & Pan, P. (2022). Multi-objective optimal design of permanent magnet eddy current retarder based on NSGA-II algorithm. *Energy Reports*, *8*, 1448–1456. https://doi.org/https://doi.org/10.1016/j.egyr.2021.11.165

Pandey, S. N., Khaliq, A., Zaka, M. Z., Saleem, M. S., Afzal, M., Zaka, Z., & Saleem, M. S. (2015). Retarder used as braking system in heavy vehicles-a review. *International Journal of Mechanical Engineering and Robotics Research*, *4*(2), 86.

Reverdin, D., & Borione, J. (1974). The electric retarder today and its future. *Mech. Eng. Publications Ltd, London*.

Talaat, M., & Mostafa, N. H. (2014, September). Use of finite element method for the numerical analysis of eddy current brake. In 15th International Workshop on Research and Education in Mechatronics (REM) (pp. 1-7). IEEE.

Sharif, S., Faiz, J., & Sharif, K. (2012). Performance analysis of a cylindrical eddy current brake. *Electric Power Applications, IET*, *6*, 661–668. https://doi.org/10.1049/iet-epa.2012.0006

Sharif, S., & Sharif, K. (2009). Influence of skin effect on torque of cylindrical eddy current brake. *2009 International Conference on Power Engineering, Energy and Electrical Drives*, 535–539. https://doi.org/10.1109/POWERENG.2009.4915143

Simeu, E., & Georges, D. (2016). Modeling and control of an eddy current brake. *Control Engineering Practice*, *4*(1), 19–26. https://doi.org/https://doi.org/10.1016/0967-0661(95)00202-4

Srivastava, R. K., & Kumar, S. (2009). An Alternative Approach for Calculation of Braking Force of an Eddy-Current Brake. *IEEE Transactions on Magnetics*, *45*(1), 150–154. https://doi.org/10.1109/TMAG.2008.2006993

Tian, J., Li, D., & Ye, L. (2020). Study on Braking Characteristics of a Novel Eddy Current-Hydraulic Hybrid Retarder for Heavy-Duty Vehicles. *IEEE Transactions on Energy Conversion*, *35*(3), 1658–1666. https://doi.org/10.1109/TEC.2020.2978304

Wu, R., Song, D., & Wu, W. (2009). The performance evaluation of electromagnetic eddy current retarder. *3rd International Symposium on Intelligent Information Technology Application, IITA 2009*, *1*, 423–425. https://doi.org/10.1109/IITA.2009.373

Ye, L., Li, D., Ma, Y., & Jiao, B. (2011). Design and Performance of a Water-cooled Permanent Magnet Retarder for Heavy Vehicles. *IEEE Transactions on Energy Conversion - IEEE TRANS ENERGY CONVERS*, *26*, 953–958. https://doi.org/10.1109/TEC.2011.2157347

Ye, L., Liu, Y., & Li, D. (2019). Performance analysis and optimization of liquid-cooled and flywheel-type eddy current retarder. *IEEE Transactions on Magnetics*, *55*(6), 1–5.

Zhang, K., Li, D., Du, X., & Zheng, R. (2014). Numerical analysis and experimentation of a novel self-excited and liquid-cooled eddy current retarder. *IEEE Transactions on Energy Conversion*, *29*(1), 196–203.

Zhou, Q., Guo, X., Tan, G., Shen, X., Ye, Y., & Wang, Z. (2015). Parameter Analysis on Torque Stabilization for the Eddy Current Brake: A Developed Model, Simulation, and Sensitive Analysis. *Mathematical Problems in Engineering*, *2015*, 10. https://doi.org/10.1155/2015/436721

APPENDIX

Appendix A: Iteration results for analysis of braking torque

Table A- 1: Analysis of braking torque for the first iteration

S. No.	Current(A)	Speed (RPM)	Braking torque (KNm)
1	6.3	601	74.26
2	6.91	662	76.65
3	8.24	757	88.36
4	8.24	882	88.69
5	8.99	968	98.98

Table A- 2: Analysis of braking torque for the second iteration

S. No.	Current(A)	Speed (RPM)	Braking torque (KNm)
1	7.2	690	79.7
2	6.9	760	87.6
3	7.0	898	98.4
4	7.4	934	81.7
5	8.3	969	89.3

Table A- 3: Analysis of braking torque for the 15th iteration

S. No.	Current(A)	Speed (RPM)	Braking torque (KNm)
1	8.7	940	84.6
2	8.6	980	87.8
3	8.4	970	89.5
4	8.8	880	98.6
5	9.0	960	89.5

Appendix B: MATLAB code for PSO

```
clc
clear all
Max_iterations=20;  % Maximum Number of Iterations
correction_factor = 2.0; % Correction factor
inertia = 1.0; % Ineritia Coeffecient
swarm_size = 5; % Number of particles
LB=[-5.12 -5.12]; % Lower Boundaries
UB=[5.12 5.12];   % Upper Boundaries
xrange=UB(1)-LB(1);
yrange=UB(2)-LB(2);
% Initial Positions
swarm(:, 1, 1)=rand(1,swarm_size)*xrange+LB(1);
swarm(:, 1, 2)=rand(1,swarm_size)*yrange+LB(2);
% Initial best value so far
swarm(:, 4, 1) = 1000;
% Initial velocity
swarm(:, 2, :) = 0;
for iter = 1 : Max_iterations

    % Calculating fitness value for all particles
    for i = 1 : swarm_size
        swarm(i, 1, 1) = swarm(i, 1, 1) + swarm(i, 2, 1)/1.3;     %update x position
        swarm(i, 1, 2) = swarm(i, 1, 2) + swarm(i, 2, 2)/1.3;     %update y position
        % The fitness function (DeJong) F(x,y)=x^2+y^2
        Fval = (swarm(i, 1, 1))^2 + (swarm(i, 1, 2))^2;          % fitness evaluation
        % If the fitness value for this particle is better than the  % best fitness value of that
particle exchange both values
        if Fval < swarm(i, 4, 1)                 % if new position is better
            swarm(i, 3, 1) = swarm(i, 1, 1);    % Update the position of the first dimension
            swarm(i, 3, 2) = swarm(i, 1, 2);    % Update the position of the second dimension
```

```
        swarm(i, 4, 1) = Fval;            % Update best value
      end
    end

    % Search for the global best solution
    [temp, gbest] = min(swarm(:, 4, 1));       % global best position

    % Updating velocity vectors
    for i = 1 : swarm_size
      swarm(i, 2, 1) = rand*inertia*swarm(i, 2, 1) + correction_factor*rand*(swarm(i, 3, 1) - swarm(i, 1, 1)) + correction_factor*rand*(swarm(gbest, 3, 1) - swarm(i, 1, 1));   %x velocity component
     swarm(i, 2, 2) = rand*inertia*swarm(i, 2, 2) + correction_factor*rand*(swarm(i, 3, 2) - swarm(i, 1, 2)) + correction_factor*rand*(swarm(gbest, 3, 2) - swarm(i, 1, 2));   %y velocity component
    end
    % Store the best fitness valuye in the convergence curve
    ConvergenceCurve(iter,1)=swarm(gbest,4,1);
    disp(['Iterations No. ' int2str(iter) ' , the best fitness value is ' num2str(swarm(gbest,4,1))]);
end
% Plot convergence curve
plot(ConvergenceCurve,'r-')
title('Convergence Curve')
xlabel('Iterations')
ylabel('Fitness Value')
```